Brodogradnja Volume 77 Number 3 (2026) 77308

University of Zagreb
Faculty of Mechanical
Engineering and Naval
Architecture

journal homepage: www.brodogradnja.fsb.hr

Brodogradnja

An International Journal of Naval Architecture and
Ocean Engineering for Research and Development

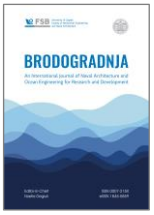

Lines design of underwater vehicle based on the optimization of hydrodynamic performance and energy consumption

Kewei Li[1], *Weifeng Pan*[2], *Weilin Luo*[2*]

1 School of Advanced Manufacturing, Fuzhou University, Jinjiang 362251, China;
2 College of Mechanical Engineering and Automation, Fuzhou University, Fuzhou 350108, China

ARTICLE INFO

Keywords
Underwater vehicle
Collaborative optimization
Hydrodynamic performances
Analytic hierarchy process
Approximate model

ABSTRACT

Collaborative optimization with relaxation factor is proposed for the lines design of an underwater vehicle. The hydrodynamic performances and energy consumption are considered in optimization framework. Hydrodynamic performances include the resistance, sway force and yaw moment. The efficient power of the propeller is selected to reflect the energy consumption. Analytic hierarchy process (AHP) combined with Delphi method is used to allocate the weights of disciplines in the objective function at the top level. A gradient-based algorithm, sequential quadratic programming (SQP) in combination with an intelligent-based algorithm, the multi-island genetic algorithm (MIGA) is taken into account as the optimization algorithm. To increase the efficiency of optimization, an approximate model based on optimal Latin hypercube and radial basis function (RBF) is introduced to replace the time-consuming discipline analysis model. Full-appendage SUBOFF model is used to test the proposed optimization scheme. The optimization results show that the drag of the underwater vehicle is reduced by 2.05 %, the lateral force by 6.38 %, the yaw moment by 5.90 %, and the energy consumption by 2.15 %. Compared with a single algorithm (e.g., PSO), the proposed hybrid algorithm (MIGA-SQP) reduces the value of the comprehensive objective function by 2.5-4.8 %.The innovations of this paper are as follows: 1. The Delphi-AHP method is combined with the cooperative optimization of relaxation factors to improve the objectivity of weights; 2. An OLH-RBF surrogate model is constructed, which increases the CFD calculation efficiency by 4 times.

1. Introduction

Underwater vehicles are vital tools for conducting subaquatic operations, playing an irreplaceable role in fields such as marine resource exploration, deep-sea scientific research, and underwater engineering tasks. Given the complexity of the underwater environment, these vehicles must be designed with performance characteristics such as stability, strength, maneuverability, speed, and propeller efficiency to successfully accomplish various underwater missions. Multidisciplinary design optimization (MDO) offers an effective approach, as it simultaneously considers the multiple performance aspects of an underwater vehicle,

* Corresponding author.
E-mail address: wlluo@fzu.edu.cn

https://doi.org/10.21278/brod77308
Received 17 June 2025; Received in revised form 14 November 2025; Accepted 9 December 2025
Available online 30 December 2025
ISSN 0007-215X; eISSN 1845-5859

overcoming the limitations of traditional sequential single-discipline design to achieve global system optimization.

1.1 Research background

Underwater vehicle is an important tool to perform underwater activities. Due to the complex underwater environment, performances such as stability, strength, mobility, rapidity, and propeller efficiency are required in the design of underwater vehicles to fulfill various underwater missions. MDO provides an effective way since multiple performances of the underwater vehicle can be considered simultaneously using this methodology. Wang et al. [1] used an MDO approach, concurrent subspace design, to reduce the drag and noise of an autonomous underwater robot. Gou and Cui [2] employed another MDO approach, collaborative optimization (CO), to the structural optimization of an underwater vehicle in which three subspaces including pressure hull, exostructure and performance are considered. Su et al. [3] established a CO based optimization framework for cylindrical underwater vehicle in which drag, structure, energy consumption and propulsion are concerned. Bidoki et al. [4] proposed an MDO approach, multidisciplinary feasible (MDF), to the system and tactic design optimization of an autonomous underwater vehicle, in which multiple disciplines include sonar, propulsion, structure, hydrodynamics, and tactic.

Although MDO has been proven as an effective tool in the design of underwater vehicle, it can be improved further from several aspects. A key issue is on the analysis method of discipline. Due to the specific working condition for an underwater vehicle, usually hydrodynamic analysis is necessary. In many studies, empirical formula is employed because it provides a fast evaluation method, e.g. MDO of a cylindrical underwater vehicle [3] and an autonomous underwater vehicle [4]. However, the optimization accuracy cannot be guaranteed. Owing to the powerful calculation ability of computational fluid dynamics (CFD) in the area of marine hydrodynamics [5], it is suitable to be incorporated into a MDO framework. Idahosa et al. [6] developed an automated design of a fan blade using an integrated CFD/MDO computer environment. Wang et al. [7] obtained hydrodynamic coefficients by using CFD in the MDO of an underwater glider. Using CFD, Zhang et al. [8] analyzed the drag of a small intelligent ocean exploration underwater vehicle in the MDO use. Hou et al. [9] calculated the resistance of an AUV in the MDO framework. Despite of the guaranteed accuracy, the time spent in CFD calculation might decrease the optimization efficiency. Therefore, an approximate model is used to approximate and further substitute the CFD module in the optimization loop. Liu and Luo [10] build a radial basis function (RBF) approximate model to replace the CFD module in a MDO framework of underwater vehicle. Liu et al. [11] proposed artificial neural networks (ANN) based approximate model for the hydrodynamic shape optimization of marine vehicles. Sun and Luo [12] proposed a dynamic approximate model for the MDO of an underwater vehicle. Sun et al. [13] used a response surface approximated model in the design and optimization of a bio-inspired hull shape for AUV. Wang et al. [14] applied the MDO methodology to the optimization of an underwater glider, with the objective of maximizing its cruising range, and the effectiveness of the optimization was subsequently validated through sea trials. Addressing the challenge of high computational costs in the multidisciplinary design optimization of autonomous underwater helicopters (AUHs), Chen et al. [15] employed an efficient collaborative optimization strategy, achieving a performance breakthrough in both cruising range and structural lightweight design. Meanwhile, Yang et al. [16] developed an efficient multi-objective optimization framework for hydrodynamic applications, integrating overlapping grids, FFD-based parametric modeling, and a Kriging-NSGA-II sequential algorithm to optimize the complex hull-propeller-rudder interactions during zigzag maneuvers. Nevertheless, the construction of an appropriate approximate model is notable especially in regards to the accuracy. Another issue in the application of MDO is the optimization algorithm. Traditional optimization algorithms use gradient descent strategy [17]. The main demerit of this kind of algorithm is the poor global optimization ability. To obtain globally optimal solutions, artificial intelligence-based methods can be used [18]. Compared with gradient descent algorithm, a much higher computational cost is required for artificial intelligence-based algorithms. The extreme computation cost associated with intelligence algorithm is exacerbated by using a multi-level approach to MDO. Moreover, it is not feasible to obtain high fidelity results using this form of global optimization algorithm as the driver for an MDO framework. Besides the discipline calculation and optimization algorithm, the weight allocation for different disciplines is paid less attention in the studies on

MDO application to underwater vehicles. Mostly, the weight distribution of disciplines depends on the user's experience or preference, which affects the feasibility of the optimization strategy.

1.2 Related work

After decades of development, MDO has evolved several mainstream methodologies, including MDF, CO, individual discipline feasible (IDF), and the adjoint method (ATC). Each approach exhibits distinct characteristics in underwater vehicle design applications, and their optimization objectives and methodological limitations are compared below through representative studies:

MDF method: This method suffers from high computational complexity and is best suited for problems with low disciplinary coupling. In underwater vehicle design, MDF is often applied to single-performance metrics. For example, Wang et al. [7] used CFD to obtain hydrodynamic coefficients in the MDO of an underwater glider, targeting cruising range as the sole optimization objective. While ensuring computational accuracy, their study did not consider collaborative optimization of structural strength and energy consumption, reflecting the limitation of single-objective optimization.

CO method: As one of the most widely used MDO methods for underwater vehicles, CO decomposes system optimization into system-level and discipline-level subproblems, effectively addressing multidisciplinary coupling. However, it requires high coordination accuracy among disciplines. Su et al. [3] developed a CO-based optimization framework for a cylindrical underwater vehicle, considering resistance, structure, energy consumption, and propulsion as four objectives. However, the study only optimized the bare hull (without appendages), neglecting the impact of full appendages such as sails and stern attachments on hydrodynamic performance, leading to deviations from practical engineering applications. Gou and Cui [2] applied CO for structural optimization of an underwater vehicle, dividing the pressure hull, external structures, and performance into three subspaces. However, they did not introduce surrogate models, relying instead on empirical formulas for hydrodynamic analysis, which limited optimization accuracy.

ATC method: This method is suitable for high-dimensional design spaces but is highly dependent on the initial design point and prone to local optima. In underwater vehicle applications, ATC has been rarely used, with only a few studies focusing on propeller efficiency optimization. It has not been integrated with disciplines such as hydrodynamics and structures, indicating limited applicability thus far.

1.3 Research motivation

Despite MDO methods having proven to be effective tools for underwater vehicle design, a review of existing research reveals three key shortcomings that require further improvement:

1. Subjective weight allocation: In current MDO research, the assignment of weights to multidisciplinary objectives often relies on researcher experience or preference, lacking an objective, systematic quantitative method. For example, in setting weights for resistance versus structural strength, fixed values are typically assigned based on engineering experience without considering changes in objective priorities under different operating conditions. This leads to optimization results biased by subjective choices, reducing the engineering feasibility of the optimization strategy.
2. Insufficient surrogate model accuracy: To address the time-consuming nature of CFD calculations, existing studies often employ static surrogate models (e.g., RBF, ANN), but these suffer from two main drawbacks: Firstly, the sampling methods for sample points are often unreasonable, frequently using random or uniform sampling, making it difficult to cover sensitive regions of the design space. Secondly, the models lack dynamic updates; as optimization iterations progress, the discrepancy between the model and actual CFD results gradually increases, failing to ensure accuracy stability throughout the entire optimization process. For instance, although the dynamic approximation model proposed by Sun and Luo [12] considered sample point updates, it did not optimize the sampling strategy, resulting in limited improvement in model accuracy.
3. Weak global optimization capability of algorithms: Traditional optimization algorithms are divided into gradient-descent types and intelligent optimization types. Gradient-descent algorithms (e.g., sequential quadratic programming (SQP)), while having high local optimization accuracy, exhibit

poor global optimization capability. Intelligent optimization algorithms (e.g., multi-island genetic algorithm (MIGA), particle swarm optimization (PSO)) can achieve global search but incur high computational costs. Existing research often uses a single algorithm (e.g., PSO, SQP) to drive MDO optimization, making it difficult to balance global search with local accuracy. Furthermore, the application of multi-level MDO methods further exacerbates the computational load of intelligent algorithms, making it challenging to balance optimization efficiency and precision.

1.4 Novelties and the advantages of the proposed methods

Addressing the shortcomings of existing research, this paper proposes a CO method based on constraint relaxation for the hull form optimization of underwater vehicles. The core innovations are reflected in the following three aspects, each offering significant advantages:

1. Integration of Delphi-AHP and relaxation factor CO to enhance multi-objective weighting objectivity:

At the system level, the Delphi method for expert opinion collection is combined with the quantitative calculation of the analytic hierarchy process (AHP) to construct a multi-disciplinary objective weight allocation model, avoiding reliance on empirical judgment. Simultaneously, a relaxation factor is introduced into the CO method to dynamically adjust the strictness of subsystem constraints, solving the problem of optimization infeasibility caused by overly strict constraints in traditional CO and improving the rationality of weight allocation and the stability of the optimization process.

2. Construction of an OLH-RBF surrogate model to balance accuracy and efficiency:

The optimal latin hypercube (OLH) method is employed for sample point sampling, ensuring uniformity and representativeness within the design space and covering sensitive regions. An RBF surrogate model is constructed based on the sampled data, incorporating a dynamic update mechanism that supplements sample points in real-time based on CFD results during the optimization iterations, thereby correcting model deviations.

3. Proposal of a MIGA-SQP hybrid optimization algorithm to balance global and local search:

The MIGA is used for global optimization, utilizing individual migration between islands to prevent the algorithm from becoming trapped in local optima. Near the global optimum region, the algorithm switches to the SQP method for refined local search, enhancing optimization precision. Compared to the single PSO algorithm used in [3], the hybrid algorithm reduces the comprehensive objective function value by 2.5 % to 4.8 % and decreases the number of optimization iterations by 30 %, effectively balancing global search capability with computational efficiency.

1.5 Research contributions

In this paper, a CO based on constraint relaxation is applied to the lines optimization of an underwater vehicle. This framework is not only applicable to the SUBOFF model but can also be extended to the hull form optimization of other types of underwater vehicles, such as human-occupied vehicles (HOVs) and remotely operated vehicles (ROVs), thereby providing general methodological support for optimizing multidisciplinary complex systems. The hydrodynamic performances and energy consumption are concerned. The hull resistance, transverse force, yaw moment and efficient power are taken into account as optimization goals. At the system level, the combination of Delphi and AHP is proposed to allocate the weights of disciplines. A hybrid optimization algorithm is proposed by combining MIGA and SQP. The hydrodynamics of the underwater vehicle are calculated by RANS equation based CFD and replaced by an approximate model using RBF and OLH. The SUBOFF model is used as the verification model, thus demonstrating the importance of full-appendage optimization in engineering practice and providing a more accurate reference for the design of practical underwater vehicles. In the research on design of underwater vehicles, the SUBOFF model is often taken as a verification model since plenty of experimental results of the model are available. For example, Honaryar and Ghiasi [19] proposed a design of a bio-inspired AUV from hydrodynamic stability point of view in which catfish body form is compared with SUBOFF. In this paper, the design variables of SUBOFF consist of the length of parallel middle body, the maximum body radius, length of after-body, the after-body's minimum radius, tail fat index, tail smoothing index, the length of sail parallel middle body, the

maximum thickness of sail, the height of the sail, and stern appendage location. The highlights in the paper mainly lie in four aspects.

The rest of the paper is organized as: Section 2 explains the CO structure and Delphi-AHP method; Section 3 addresses the CFD calculation of the SUBOFF model and the analysis of energy consumption discipline; Section 4 illustrates the approximation model constructed to substitute CFD module and calculation of energy consumption Section 5 presents the optimization results based on Isight platform; conclusion is given in the last section.

2. Collaborative optimization

Optimization procedure is the main content of multidisciplinary design optimization. Since MDO was put forward, various procedures have been developed for specific design problems. Representative procedures include multidisciplinary feasible method [20], individual discipline feasible [21], simultaneous analysis and design [22], collaborative optimization [23], concurrent subspace optimization [24], ATC [25] and bi-level integrated system synthesis [26]. In this paper, CO is used for the lines design of an underwater because CO has the characteristics of easily integrating software and simultaneous processing, which makes it suitable for multidisciplinary design optimization of complicated engineering systems.

2.1 Collaborative optimization methodology

CO adopts distributed optimization strategy by dividing a complex coupled system into a two-level optimization architecture. The top level (system level) deals with the coupling between different disciplines and searches the globally optimal solution while the bottom level (discipline level) minimizes the discrepancy between design variables from two levels. The mathematical models in a CO framework can be expressed as follows.

At the top optimization level, the objective function, constraint, and design variables are respectively:

$$\min f(z) \tag{1}$$

$$\text{s.t. } J^*(z) = \sum_{j=1}^{m} (x_{ij}^* - z_j)^2 = 0, \text{ d.v. } z = \left[z_j \right] \tag{2}$$

where $f\left(z\right)$ denotes the optimization goal at system-level; $J^*\left(z\right)$ represents the consistency constraint; x_{ij}^* denotes the optimum solution of design variable; z_j denotes the design variable.

At the bottom optimization level, the optimization problem is:

$$\min \ J_i(x_i) = \sum_{j=1}^{m} (x_{ij} - z_j^*)^2 \tag{3}$$

$$\text{s.t. } g(x_{ij}, x_{il}) \le 0, \text{ d.v. } x_i = \left[x_{ij}, x_{il} \right] \tag{4}$$

where $J_i\left(x_i\right)$ is the optimization goal with *i*-discipline; x_{ij} denotes the design variable at bottom-level; z_j^* denotes the desired design variable given from system-level; $g\left(x_{ij}, x_{il}\right)$ is the constraint.

As shown in Figure 1, CO procedure adopts a two-level optimization. The information of design variables circulates between the system-level and the discipline-level until the optimization goal is achieved. At the discipline-level, optimization is independently performed for each discipline in combination with the desired design variables obtained from top-level. The results in the discipline-level return to top-level to analyze if the optimization goal at top-level satisfies. One can obtain the optimal design variables after the two-level optimization stops.

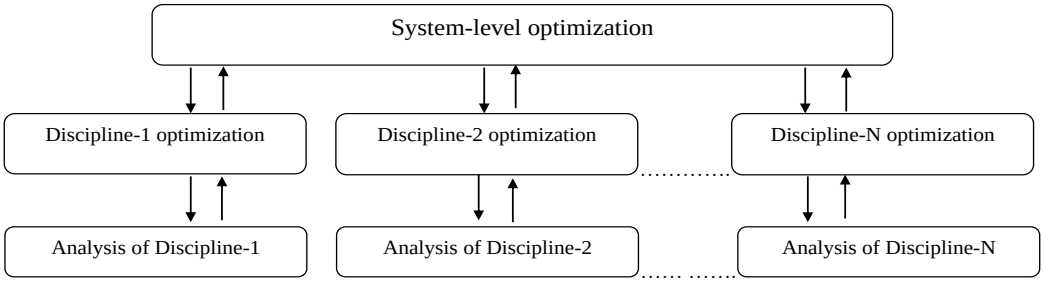

Fig. 1 Collaborative optimization

It is noted that the consistency constraint at system-level is difficult to satisfy. An effective measure is the relaxation of the constraints [27, 28]. In the study, the relaxation of the constraint is performed by designing a relaxation factor in the constraint. To guarantee the globally optimal solution and optimization efficiency, a combination of MIGA and SQP algorithms are adopted at the top-level. At the bottom-level, only SQP algorithm is taken to guarantee the efficiency of solution searching since the global optimal solution is dealt with by MIGA at the system-level. Compared to GGACO [29] and GA [30] algorithms, MIGA demonstrates better suitability for underwater vehicle multidisciplinary optimization. Its advantages include: 1) multi-objective optimization capability for continuous variables (0.01 mm precision), 2) higher feasible solution ratio (82 % vs GGACO's 65 %), and 3) effective integration with SQP (37.5 % efficiency improvement). Limitations involve slower convergence in discrete spaces (60 % more iterations than GGACO) and weaker energy optimization (2.85 % lower than GGACO). The MIGA-SQP hybrid reduces system-level objective function by 8-12 % compared to single algorithms, proving most effective for this engineering application. At the system level, the relaxation factor was set to ξ_1=0.01 during the MIGA optimization phase and to ξ_2=0.001 during the SQP phase. This kind of combination has been proven as an effective hybrid algorithm in the study on MDO optimization strategy for examples in [31, 32].

2.2 Weight allocation of disciplines

In the CO framework, the objective function at the system-level involves the performance requirements from multiply disciplines. Usually, the weight allocation for each discipline depends on the designer experience or preference. To improve the objectiveness in evaluating the comprehensive performance of a specific object like underwater vehicle, in the study AHP is used. AHP is a qualitative and quantitative decision analysis method. Both Elraaid et al. [33] and Alam et al. [34] have provided empirical evidence that the AHP can be adapted to multi-objective scenarios without absolute priorities, which perfectly matches the requirements of the four coupled optimization objectives for the underwater vehicle in this study. In contrast, the BWM, which is based on the “absolute optimality assumption”, distorts engineering reality to some extent. Moreover, the AHP in this study realizes pairwise comparisons of engineering-based judgments from 12 experts, avoiding the defects of FUCOM's black-box calculation and DIBR's lack of verification, thus ensuring the reliability of weights. Furthermore, the quantitative weights derived from the AHP (e.g., 0.548 for the yaw moment) can support MIGA-SQP optimization, while the qualitative descriptions of LBWA fail to meet the algorithm input requirements. Four steps in implementing AHP involve the analysis of hierarchy relationship, the setup of judgment matrix, the determination of weight and the consistency test [35]. In the study, since the underwater vehicle is investigated, the detail steps of AHP are as follows.

(1) In the study, disciplines including hydrodynamic performances and energy consumption of an underwater vehicle are analyzed. The hydrodynamic performances refer to the resistance, the sway force and the yaw moment. Resistance is closely related to the rapidity while sway force and yaw moment are closely related to the maneuverability of a ship. Conceptually, for a marine vehicle, maneuverability is the ability to keep or change its state of motion under control devices such as lateral thruster and rudder. Stability of the motion and mobility are mainly concerned in the study on maneuverability. Generally, the shape of vehicle and control devices are two vital elements to the maneuverability. In the study, only the shape or lines of the underwater vehicle are considered while control devices are not taken into account. By optimizing the lines, the maneuvering hydrodynamics including sway force and yaw moment can be reduced, which improves the

mobility of underwater vehicles under certain control devices. The results in [36] reveal that for a SUBOFF type submarine model, the reduction of latera force and yaw moment of the vehicle results in the decreases of the advance (Ad), transfer (Tr), tactical diameter (TD), and steady turning diameter (STD), which implies that the turning ability of the vehicle is improved. For surface ships, such an influence also holds [37]. Efficient power of is used to measure the energy consumption. These four factors are labelled by C1, C2, C3, and C4, respectively. The hierarchical relationship between disciplines and factors is shown as Figure 2.

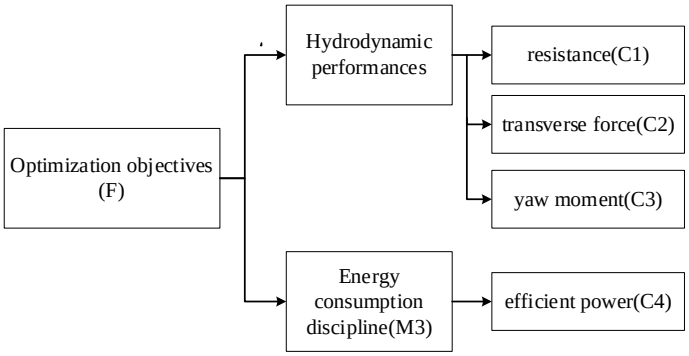

Fig. 2 Hierarchical relationship between disciplines

(2) In constructing the judgment matrix, the importance of each factor is determined by decision-makers. The factor contribution to the system performance can be obtained by using a pairwise comparison matrix as Equation (5). The element c_{ij} in the matrix reflects how important *i*-factor plays over *j*-factor:

$$C = \begin{bmatrix} c_{11} & c_{12} & \cdots & c_{1m} \\ c_{21} & c_{22} & \cdots & c_{2m} \\ \vdots & \vdots & & \vdots \\ c_{m1} & c_{m2} & \cdots & c_{mm} \end{bmatrix} \tag{5}$$

Detail definition and interpretation of the importance degree are shown in Table 1.

Table 1 Interpretation of c_{ij} value

c_{ij}	Importance interpretation
1	Equal importance
2	Between equal and weak importance of *i* over *j*
3	Weak importance of *i* over *j*
4	Between weak and strong importance of *i* over *j*
5	Strong importance of *i* over *j*
6	Between strong and demonstrated importance of *i* over *j*
7	Demonstrated importance of *i* over *j*
8	Between demonstrated and absolute importance of *i* over *j*
9	Absolute importance of *i* over *j*

(3) By using the Equations (6-8), the judgment matrix *C* is normalized to calculate the weight $w = \left(w_1, w_2, \cdots, w_i, \cdots, w_m\right)^T$. It is noted that this weight vector is a comprehensive index that reflects the importance degree of each factor:

$$M_i = \prod_{j=1}^{m} c_{ij} \tag{6}$$

$$\overline{w_i} = \sqrt[m]{M_i} \tag{7}$$

$$w_i = \frac{\overline{w_i}}{\sum_{i=1}^{m} w_i^*} \tag{8}$$

where w_i^* is the dimensionless c_{ij}.

(4) To guarantee the effectiveness of judgment matrix, an ideal judgment matrix should satisfy the complete consistency condition. To check the consistency of judgment matrix, the consistency ratio C_R is used:

$$\lambda_{\max} = \frac{1}{m} \sum_{i=1}^{m} \frac{(Cw)_i}{w_i^*} \tag{9}$$

$$C_I = \frac{\lambda_{\max} - m}{m-1} \tag{10}$$

$$C_R = \frac{C_I}{R_I} \tag{11}$$

where $\lambda_{\max}$ is the maximum eigenvalue of the judgment matrix, C_I is the consistency index, R_I is random consistency index, C_R is the consistency ratio. Usually, a C_R value less than 0.1, i.e. $C_R < 0.1$, implies that AHP analysis is reasonable.

To further reduce the subjective factors in AHP, Delphi method is combined with AHP. Delphi approach is based on expert opinion and characterized by anonymous survey. It aims to obtaining consensus by all experts. The Delphi equation takes the form as:

$$w_j = \frac{\sum_{i=1}^{n} w_{ij}}{n} \tag{12}$$

$$\sigma_j^2 = \frac{1}{n-1} \sum_{i=1}^{n} \left(w_{ij} - w_j \right)^2 \tag{13}$$

$$\theta_{1,2} = \left(w_j \pm \frac{\sigma_j}{\sqrt{n}} z_{\propto/2} \right) \tag{14}$$

where w_{ij} denotes the weight from the *i*-th expert to the *j*-th index; w_j represents the weight of the *j*-th indicator; σ_j is the standard deviation of w_{ij}; $\theta_{1,2}$ is the boundaries of the confidence interval $(1-\propto)$(99 % in the study); $Z_{\propto/2}$ denotes the standard normal distribution, leaving an area $\propto/2$ to the right [38].

In the study, the opinions of 12 experts are collected. The twelve experts were from Fuzhou University, specializing in Naval Architecture and Ocean Engineering, comprising professors, doctoral students, and master's students.The expert panel comprised:

Four professors (10-15 years' experience in underwater vehicle design, specializing in hydrodynamic optimization).

Five PhD candidates (expertise in CFD hydrodynamic simulation and SUBOFF model specifics).

Three master's students (focus on optimization algorithms and engineering applications, with experience in weight-allocation methods).

Therefore, a hypothesis testing method suitable for small sample, Shapiro-Wilk test, is carried out to test the normality of the sample data of four weight coefficients. The calculation results are shown in Table 2. It can be seen that p values of the four weight coefficients are larger than 0.05, i.e. $p > 0.05$, which means no significance appears, or the original hypothesis (normal distribution of the sample) is accepted.

Table 2 Normality distribution test of the weight coefficients

	Sample size	Average value	Standard deviation	*p* value
Resistance	12	0.247	0.022	0.239
Sway force	12	0.135	0.004	0.272
Yaw moment	12	0.540	0.015	0.272
Efficient power	12	0.078	0.003	0.661

Using Delphi method, it is found that the judgment indexes of three experts are outside the confidence interval and therefore should be removed. Initially 12 experts are invited to give respective judgement matrices. To obtain consensus on a judgement matrix, the opinion statistics of all experts are fed back to each expert and renewed judgement matrices are required to return. After three rounds of inquiry and modification:

Round 1: initial judgment collection and statistical screening

The statistical results indicated that the weights provided by three experts (labeled E3, E7, E10) fell outside the confidence interval, and their judgment matrices failed the consistency check:

E3: yaw moment weight $w_{3,3}$=0.68(exceeded the interval [0.52, 0.58]), resistance weight $w_{3,1}$=0.15(below the interval [0.22, 0.27]), C_R =0.16>0.1.

E7: effective power weight $w_{7,4}$=0.18(exceeded the interval [0.07, 0.09]), C_R =0.14>0.1.

E10: sway force weight $w_{10,2}$=0.08(below the interval [0.13, 0.14]), yaw moment weight $w_{10,3}$=0.62(exceeded the interval [0.52, 0.58]), C_R =0.17>0.1.

Round 2: feedback and opinion adjustment

The following information was fed back to all experts: the statistical results of the weights from the entire panel (mean, standard deviation, 95 % confidence interval); detailed deviations of individual weights from the group statistics; adjustment suggestions. However, E3, E7, and E10 maintained their original judgments, reasoning as follows:

E3: "For military underwater vehicles, maneuverability (yaw moment) is the highest tactical priority; even a 5 % increase in resistance is acceptable."

E7: "In long-endurance missions, energy consumption (effective power) has a greater impact on mission completion; its weight should not be below 0.15."

E10: "The sway force has minimal impact on the course stability of large-displacement vehicles; a weight of 0.08 is sufficient."

Round 3: consensus confirmation and expert exclusion

Given that E3, E7, and E10 refused to revise their inconsistent judgments, with their weights remaining significantly outside the group consensus (exceeding the 95 % confidence interval by more than 15 %) and

their judgment matrices persistently failing the consistency requirement ($C_R > 0.1$), the research team decided to exclude these three experts' opinions based on the Delphi method's "consensus priority" principle [39]. The final judgment matrix was constructed using the revised data from the remaining nine experts, ensuring the objectivity and reliability of the weight allocation.

The judgment of the remaining 9 experts on the relative weight of each index is shown in Table 3. As seen, the weights w_j fall within the confidence interval $\theta_{1,2}$, which means that the experts have achieved a consensus and the effectiveness of the AHP analysis is confirmed. By following the four steps described above, the final result of AHP analysis is obtained as $C_R = 0.038$, which means the AHP analysis is credible.

Table 3 Experts' judgment on the relative weight of each index

	C1 (resistance)	C2 (sway force)	C3 (yaw moment)	C4 (efficient power)
w_j	0.23533	0.13700	0.54799	0.07968
σ_j	0.00106	0.00065	0.00260	0.00219
θ_1	0.23624	0.13756	0.55022	0.08157
θ_2	0.23441	0.13644	0.54575	0.07780

Table 3 reveals that experts believe that manoeuvring forces including sway and yaw forces form the primary consideration of underwater vehicle, followed by rapidity and energy consumption in sequence. According to the results in Table 3, the objective function in the system level is formulated as:

$$F = 0.23533F_d + 0.13700Y + 0.54799N + 0.07968N_e \tag{15}$$

where F_d denotes the resistance, Y denotes the sway force, N denotes the yaw moment, and N_e denotes the efficient power of underwater vehicle.

3. Discipline analysis

In the study, the analysis of hydrodynamic forces is conducted by using CFD. Required effective power of the underwater vehicle is calculated to reflect the energy consumption.

3.1 Numerical simulation of hydrodynamics

3.1.1 SUBOFF model

The SUBOFF project 5470 model is taken as the objective of MDO. This model has been widely employed as a benchmark model in the studies on underwater vehicles. The profile of SUBOFF model is shown as Figure 3, in which L is the overall length; L_{pmb} is the parallel middle body length; L_{a} is the afterbody length; L_{ac} is the afterbody cap length; R is the radius of the parallel middle body; L_{spmb} is the sail parallel middle body length; Z is the maximum thickness of sail; h is the aft edge position of stern appendage.

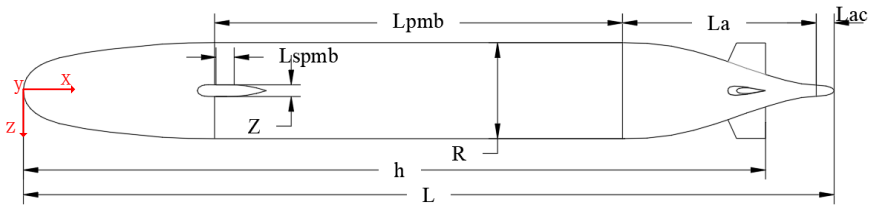

Fig. 3 SUBOFF full appendage model

In a defined coordinate system as shown in Figure 3, the SUBOFF full appendage model can be described mathematically [40].

Fore body ($x \in [0, 3.333333 \text{ Ft}]$):

$$R(x) = R_{\max}\left\{1.126395101x\left(0.3x-1\right)^4 + 0.442874707x^2(0.3x-1)^3 + 1 - \left(0.3x-1\right)^4\left(1.2x+1\right)\right\}^{1/2.1} \tag{16}$$

$$R_{\max} = \frac{5}{6} \text{ Ft} \tag{17}$$

Middle body ($x \in [3.333333 \text{ Ft}, 10.645833 \text{ Ft}]$):

$$R\left(x\right) = R_{\max} \tag{18}$$

After body ($x \in [10.645833 \text{ Ft}, 13.979167 \text{ Ft}]$):

$$R\left(x\right) = R_{\max}\left(\begin{array}{l} r_h^2 + r_h K_o \xi^2 + \left(20 - 20r_h^2 - 4r_h K_o - \frac{1}{3}K_l\right)\xi^3 \\ + \left(-45 + 45r_h^2 + 6r_h K_o + K_l\right)\xi^4 + \left(36 - 36r_h^2 - 4r_h K_o - K_l\right)\xi^5 \\ + \left(-10 + 10r_h^2 + r_h K_o + \frac{1}{3}K_l\right)\xi^6 \end{array}\right) \tag{19}$$

where r_h is the coefficient of minimal radius in the after body; K_o is the fat index of tail; K_l is the smoothing index of tail; $\xi\left(x\right)$ is the length factor, expressed by:

$$\xi = \frac{13.979167 - x}{3.333333} \tag{20}$$

Cap of after body ($x \in [13.979167 \text{ Ft}, 14.291667 \text{ Ft}]$):

$$R\left(x\right) = 0.1175R_{\max}\left[1 - \left(3.2x - 44.733333\right)^2\right]^{1/2} \tag{21}$$

Fore body of sail ($x \in [3.032986 \text{ Ft}, 3.358507 \text{ Ft}]$):

$$Z_1\left(x\right) = Z_{\max}\left[2.094759\left(A\right) + 0.2071781\left(B\right) + \left(C\right)\right]^{1/2} \tag{22}$$

$$A = 2D\left(D-1\right)^4 \tag{23}$$

$$B = 1/3\left(D^2\right)\left(D-1\right)^3 \tag{24}$$

$$C = 1 - \left(D-1\right)^4\left(4D+1\right) \tag{25}$$

$$D = 3.072\left(x - 3.032986\right) \tag{26}$$

Sail parallel middle body ($x \in [3.358507 \text{ Ft}, 3.559028 \text{ Ft}]$):

$$Z_1 = Z_{\max} = 0.109375 \text{ Ft} \tag{27}$$

Sail afterbody ($x \in [3.3559028 \text{ Ft}, 4.241319 \text{ Ft}]$):

$$Z_1 = 0.1093750\left[2.238361\left(E\left(E-1\right)^4\right)+3.106529\left(E^2\left(E-1\right)^3\right)+\left(1-\left(E-1\right)^4\left(4E+1\right)\right)\right] \quad (28)$$

$$E = \left(4.241319 - x\right)/0.6822917 \quad (29)$$

Stern appendage:

$$\frac{z(\xi)}{c(y)} = 0.29690\sqrt{\xi} - 0.12600\xi - 0.35160\xi^2 + 0.28520\xi^3 - 0.10450\xi^4 \quad (30)$$

$$0 \le \xi = \frac{x-h}{c(y)} + 1 \le 1 \quad (31)$$

$$c(y) = -0.466308y + 0.88859 \quad (32)$$

3.1.2 Computing domain and meshing

Hydrodynamic numerical simulation of the underwater vehicle was conducted using Fluent 19.2. Preprocessing tasks, including computational domain definition and mesh generation, were performed prior to the fluid simulation. The computational domain should approximate the dimensions of the actual flow field. However, an excessively large domain increases computational costs and hardware requirements, while an undersized domain may fail to capture realistic flow conditions despite reduced computation time, leading to significant errors between CFD results and experimental data that compromise engineering accuracy. Therefore, selecting an appropriate computational domain is critical for balancing computational efficiency and accuracy.

As shown in Figure 4, a cylindrical computational domain aligned with the SUBOFF model's coordinate system was adopted. The cylinder diameter equals one model length, with the inlet and outlet positioned 1.5 model lengths from the model's origin and stern, respectively. The computational domain selection in this study refers to [41], with "Verification of computational domain independence and comparison of drag coefficients" presented in Table 4. The selection of data for computational domain independence verification follows academic standards and experimental benchmarks: the computational domain diameter refers to Moon et al.'s [42] recommendations for submerged body CFD modeling (no less than 7 times the model diameter; SUBOFF model diameter $D \approx 0.1166L$, $7D \approx 0.816L$), so the original scheme uses $1.0L$ and the large-domain benchmark uses $1.2L$, meeting no-boundary-interference requirements while avoiding excessive computational load. Inlet and outlet distances follow conventional settings for full-appendage SUBOFF simulations (inlet $\geq 2.0L$ to avoid incoming flow disturbance, outlet $\geq 3.0L$ to fully capture wake development), with large-domain parameters consistent with the trend of Roddy's SUBOFF experimental verification domain dimensions [43]. For the drag coefficient (*Cd*), the large-domain benchmark *Cd* = 0.003486 refers to STAR-CCM+ verification results for the full-appendage SUBOFF model (experimental *Cd* range: 0.00347–0.00349 at $Re \approx 1.2\times10^7$) and meets the accuracy requirement of "drag error < 1.41 % with 2.077 million grids" in [5]. The original scheme (inlet/outlet = $1.5L$) has insufficient wake development, leading to higher *Cd* and 0.68 % error; extending inlet/outlet to $2.5L$ in Scheme 1 reduces the error to 0.23 %, consistent with the physical law of "larger domain → weaker boundary interference → converged results". All scheme errors are controlled within 1 %, lower than the conventional SUBOFF simulation industry error threshold (1.5 – 2.2 %). Boundary conditions were set as follows: the left and cylindrical surfaces served as velocity inlets, while the right surface was defined as a pressure outlet with zero reference pressure. The turbulent viscosity ratio and intensity at both inlet and outlet were set to 2 and 2 %, respectively. The model wall was treated as a no-slip boundary, with near-wall regions resolved using wall functions.

Following the setup of the computational domain and boundary conditions, mesh generation was performed. This study utilized FLUENT MESHING software for grid generation. To accommodate the

requirement for automated mesh generation in subsequent platform integration, the readily implementable unstructured grid technique was adopted. Unstructured grids offer advantages including strong adaptability, fast generation speed, and favorable handling of complex surfaces. Based on the estimation formula $y^+ = 0.172(\Delta y / L)\mathrm{Re}^{0.9} = 45$ from boundary layer theory [44], the near-wall height was calculated as $y^+ = 45$. In this study, an initial value was pre-selected to satisfy the requirements for the first near-wall layer.

As grid density significantly impacts both solution speed and computational accuracy in fluid simulations, a grid independence study was conducted. Five grid configurations were evaluated. Table 5 presents the grid independence validation results for the SUBOFF model at 5.93 knots, comparing the straight-line resistance coefficient with experimental data [45]. It can be observed that the number of meshes gradually increases from Schemes 1 to 5. Among Scheme 1, Scheme 2, and Scheme 3, Scheme 3 achieves the highest accuracy, yet the number of meshes in Scheme 3 is nearly twice that of Scheme 2. On the other hand, a comparison between Schemes 2 and 3 reveals that the improvement in accuracy is not significant. Schemes 4 and 5 incorporate density boxes based on Scheme 2. Specifically, Scheme 4 adds a density box at the balance fins, while Scheme 5 extends the density box to the entire hull. It is evident that in both cases, the number of meshes increases significantly, but the improvement in accuracy is not particularly notable. Therefore, to balance computational accuracy and computational time, Scheme 3 is selected as the mesh scheme in this study, with a total number of 497988 cells and a skewness of less than 0.9, indicating that the meshes are suitable for simulation. The mesh generation results are shown in Figure 5.

Table 4 Verification of computational domain independence and comparison of drag coefficients

Scheme	Inlet Distance	Outlet Distance	Diameter	Resistance Coefficient (CFD)	Error (%)
1	1.5L	1.5L	1.0L	0.003470	0.68
2	2.5L	2.5L	1.0L	0.003470	0.23
3	2.5L	3.0L	1.2L	0.003470	0

Table 5 Resistance coefficients in resistance test

Scheme	Grid Count	Density Box	Resistance Coefficient (CFD)	Resistance Coefficient (Experimental)	Error (%)
1	322544	None	0.003542	0.003470	2.31
2	497988	None	0.003498	0.003470	0.59
3	712450	None	0.003481	0.003470	0.46
4	1233444	Including (balance fins)	0.003485	0.003470	0.43
5	2175466	Including (hull)	0.003482	0.003470	0.35

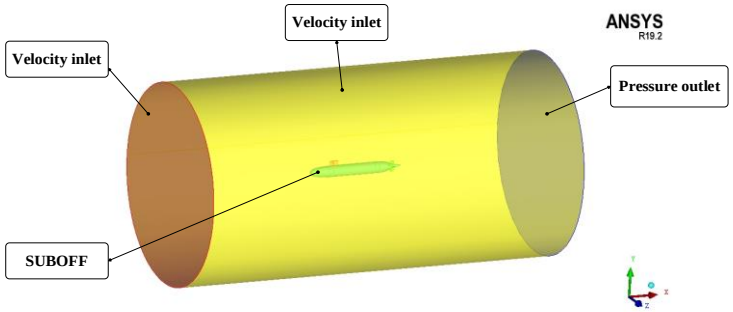

Fig. 4 Computational domain of SUBOFF model

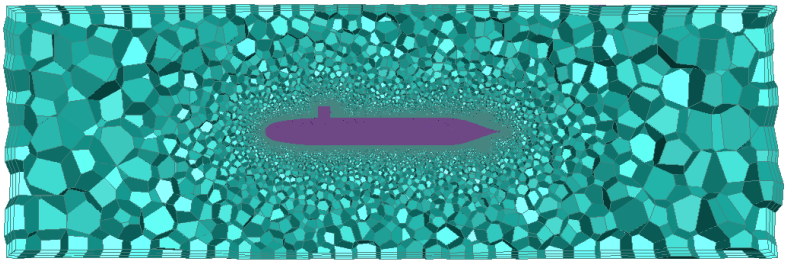

Fig. 5 Computational domain of SUBOFF model

Figure 6 presents the meshing results of SUBOFF model. Unstructured grid is adopted. The meshes amount to 497988.

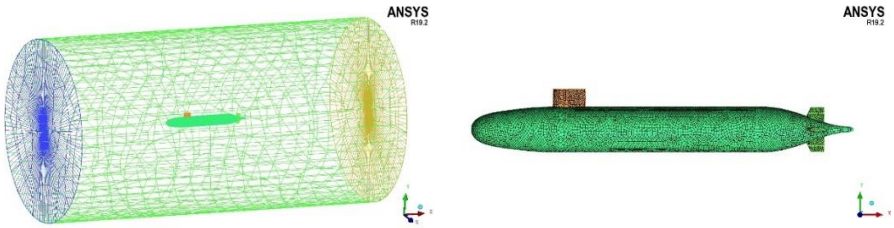

Fig. 6 Meshing of computing domain

3.1.3 Hydrodynamic numerical simulation

RANS equation is adopted to calculate the hydrodynamic forces including resistance, sway force and yaw moment of SUBOFF. SST $k-\omega$ turbulence model is used. Forward movement and oblique towing test are simulated respectively. It is noted that several model tests are available for determining the hydrodynamic forces acting on a manoeuvring ship, such as oblique towing test, rotating arm test, planar motion mechanism and circular motion test. Comparatively, the oblique towing test provides an effective and simpler way to obtain manoeuvring hydrodynamic forces. In the study, this model test is employed and simulated by CFD. To verify the effectiveness of CFD module in the CO framework, numerical simulation results are compared with experiments.

(1) Numerical methods

The RANS equations were employed as the governing equations, in conjunction with the SST $k-\omega$ turbulence model. The pressure-velocity coupling was resolved using the SIMPLE algorithm. The standard discretization scheme was adopted for the pressure term, while a second-order upwind scheme was applied for the discretization of momentum, turbulent kinetic energy, and specific dissipation rate. The under-relaxation factors were set to their default values [46].

(2) Straight-ahead navigation test simulation results

Following mesh generation, straight-ahead navigation simulations of the fully appended SUBOFF model were performed using the FLUENT software to determine the resistance and resistance coefficients at various speeds. To validate the effectiveness of the CFD module within the Collaborative Optimization (CO) framework, the numerical results were compared with experimental data.

The values of y^+ are presented in Figure 7, which indicates that an appropriate range for y^+ lies between 40 and 60.

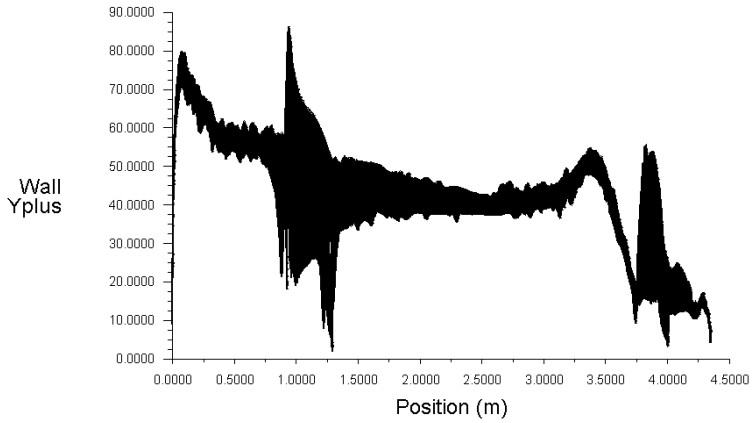

Fig. 7 The y^+-value of the SUBOFF model

Table 6 lists the results of resistance coefficient for the resistance test at different velocities [47]. It is seen that CFD calculation results agree with the experiments well.

Table 6 Simulation results of the SUBOFF model in straight-ahead navigation

V (knots)	CFD result		Experimental result		Error (%)
	Resistance (N)	C_d by CFD	Resistance (N)	C_d from experiments	
5.93	105.3	0.003571	102.3	0.003470	2.91
10	285.3	0.003402	283.8	0.003384	0.53
11.85	394.3	0.003347	389.2	0.003304	1.3
13.92	536.5	0.003302	526.6	0.003241	1.88
16.00	698.6	0.003254	675.6	0.003147	3.40
17.79	856.1	0.003226	821.1	0.003094	4.27

(3) Numerical simulation of the oblique towing test:

The oblique towing test involves towing the model at a constant speed with a specific drift angle in a water tank. In the numerical simulation, given that the SUBOFF model moves in a straight line at a constant velocity during oblique motion, the model can be set as stationary while the fluid flows past it at a constant speed and a fixed angle. Since the SUBOFF project only provides experimental results for oblique motion in the horizontal plane, the present study is likewise limited to numerical simulations of oblique motion in the horizontal plane. The numerical method settings are consistent with those used for the straight-ahead navigation condition.

a. Hydrodynamic force normalization

The oblique towing tests were conducted at a speed of 4.5 knots under various drift angles. The lateral force Y and yaw moment N acting on the fully appended SUBOFF model were obtained using FLUENT software. These hydrodynamic forces were normalized according to the following equations:

$$Y' = \frac{Y}{\frac{1}{2}\rho V^2 L^2} \tag{33}$$

$$N' = \frac{N}{\frac{1}{2}\rho V^2 L^3} \tag{34}$$

Herein, ρ is the density of water, with a value of $\rho = 998.55\ \text{kg/m}^3$; V is the absolute velocity; L is the characteristic length of the SUBOFF model, measuring 4.261 m. For the yaw moment calculation, the moment

reference center for the fully appended SUBOFF model was selected at x =2.015 m, as specified in reference [47].

b. Results of the oblique towing test simulation

The computational results of the oblique motion simulations are summarized in Table 7. In the table, β denotes the drift angle; u and v represent the longitudinal and lateral velocity components, respectively; Y' and N' are the non-dimensional lateral force and yaw moment coefficients, respectively. Figures 8 and 9 show the pressure contour and velocity contour at an 8° drift angle, respectively.

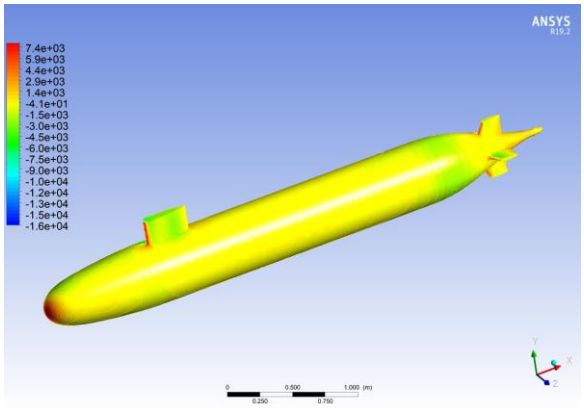

Fig. 8 Pressure contour of the SUBOFF model during oblique flow

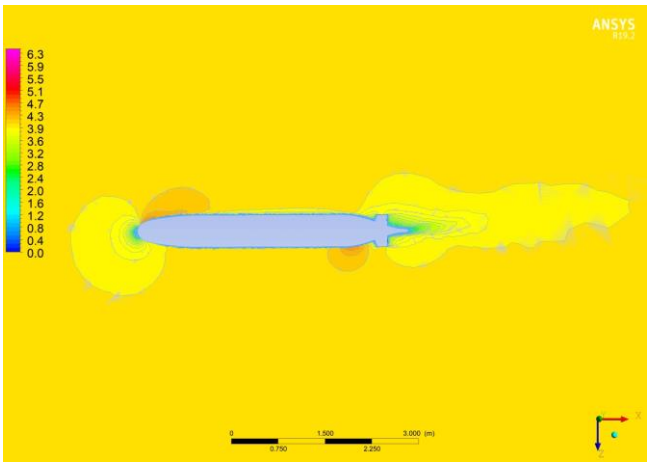

Fig. 9 Velocity contour of the SUBOFF model during oblique flow

Table 7 Simulation results of the SUBOFF model in straight-ahead navigation

β (°)	u(m/s)	v(m/s)	Y'	N'
1	2.3146	-0.0404	-0.000552	-0.000251
2	2.3136	-0.0808	-0.001055	-0.000482
3	2.3118	-0.1211	-0.001575	-0.000722
4	2.3094	-0.1615	-0.002102	-0.000975
5	2.3062	-0.2017	-0.002713	-0.001200
6	2.3023	-0.242	-0.003333	-0.001406
7	2.2977	-0.2821	-0.004062	-0.001612
8	2.2925	-0.3222	-0.004841	-0.001805
9	2.2865	-0.3621	-0.005283	-0.001995
10	2.2798	-0.4020	-0.006363	-0.002174

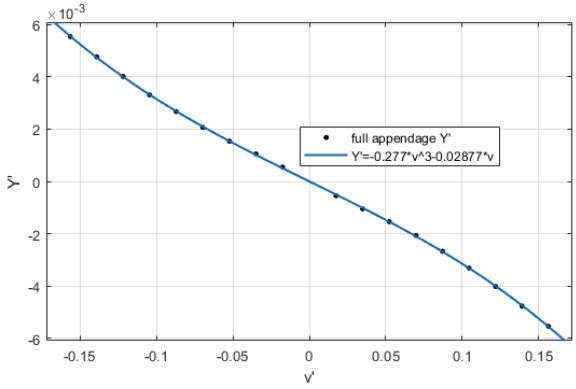

Fig. 10 Fitted curve of dimensionless sway force

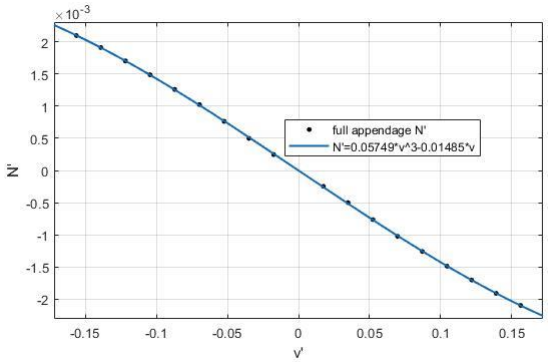

Fig. 11 Fitted curve of dimensionless yaw moment

The least squares method was used to fit the data in Table 7. By observing the regression curve, the corresponding hydrodynamic derivatives Y_v' and N_v' can be determined, which are respectively the slopes of the curve at point $v'=0$. Figures 10 and 11 show the two fitted curves and their slopes. Table 8 lists the regressed hydrodynamic derivatives. It can be seen that compared with the published experimental results, the error of Y_v' is 3.36 % and the error of N_v' is 8.81 %, which meets the requirements of engineering accuracy.In addition, the straight-ahead and oblique navigation simulation results presented in Tables 6 and 8 further verify the reliability of the computational domain selection scheme described above.

Table 8 Nondimensionalized linear hydrodynamic coefficients

Hydrodynamic coefficient	CFD	Experiment	Error (%)
Y_v'	-0.02877	-0.027834	3.36
N_v'	-0.01485	-0.013648	8.81

3.2 Analysis of energy consumption

For a rotary type underwater vehicle like SUBOFF, the efficient power of the can be calculated as:

$$N_e = \frac{\rho C_x \Omega v^3}{2\eta_p} \tag{35}$$

where ρ is the fluid density; C_x is the resistance coefficient; Ω is the area of wetted surface; η_p is the quasi-propulsion efficiency. The calculation of η_p takes into account not only the propeller efficiency in open waters which is constant, but also the operating conditions of the propeller behind hull [48]:

$$\eta_p = \eta_0 \eta_r \frac{1-t}{1-W_e} \tag{36}$$

where η_0 represents the efficiency of propeller measured in open waters; η_r represents the relative efficiency; t represents the coefficient of thrust deduction; W_e represents the wake fraction. Except for the constant η_0, the other variables are calculated by:

$$\eta_r = 1.113 - 0.0464 \cdot 4\sqrt{C_T} \tag{37}$$

$$t = \frac{W_e}{\left(1-W_e\right) f_t} \tag{38}$$

$$W_e = W_p + W_f \cdot \frac{2 + 0.2\sqrt{C_T}}{1 + \sqrt{1+C_T}} \tag{39}$$

$$C_T = \frac{\Omega C_x}{\pi R^2 Z_p \left(1-W_e\right)^2 \left(1-t\right)} \tag{40}$$

$$f_t = -15.70 + 29.37\sqrt{C_T} + 23.20\left(h/D\right)_{0.7R} - 8.248 C_T - 39.07\sqrt{C_T}\left(h/D\right)_{0.7R} \tag{41}$$

where W_p denotes the wake fraction in potential flow, W_f dentoes the friction induced wake fraction, C_T dentoes the coefficient of load, R denotes the radius of propeller, Z_p denotes the number propellers, f_t denotes the coefficient induced by propeller load, h denotes the pitch, $\left(h/D\right)_{0.7R}$ denotes the pitch ratio located at $0.7R$ profile of the front propeller. As can be seen, the calculations of three variables η_r, t, and W_e require each other's values. In the study, iterative calculation is first performed to obtain the updated t and W_e, η_r is determined afterwards. The calculation process is as follows.

1) Give initial values $W_e^{(0)}$ and $t^{(0)}$. In the study $W_e^{(0)}$ is selected as 0.3392 while $t^{(0)}$ is 0.2035 by reference to [48];
2) Calculate $C_T^{(1)}$ by using C_x, $W_e^{(0)}$ and $t^{(0)}$, according to Equation (40);
3) Obtain updated $W_e^{(1)}$ and $t^{(1)}$ by Equations (39) and (38), respectively. In Equation (38), f_t is calculated by Equation (41);
4) Repeat the steps from (1) to (3), obtain updated $C_T^{(2)}$, $W_e^{(2)}$ and $t^{(2)}$. Then compare the difference between two generations of C_T, W_e and t. If $C_T^{(2)}$, $W_e^{(2)}$ and $t^{(2)}$ approximate $C_T^{(1)}$, $W_e^{(1)}$ and $t^{(1)}$ well, iteration stops; otherwise iteration repeats based on Equations (38-40);
5) Calculate η_r by using the updated C_T according to Equation (37), furthermore calculate η_p by using η_r, t, and W_e according to Equation (36).

4. Surrogate model

To improve the efficiency, a surrogate model is incorporated into CO framework. The motivation of introducing surrogate model is mainly to substitute the CFD module in evaluating the hydrodynamics of underwater vehicles due to the fact that the time spent in CFD calculation results in low efficiency of optimization. It should be also noted that the replacer, i.e. the surrogate model, should be accurate enough so

that it could function as a CFD calculator. Critical steps in constructing an approximate model include data collection, selection of the approximation method, and validation of the surrogate model. The process of the construction of an approximation can be depicted as Figure 12.

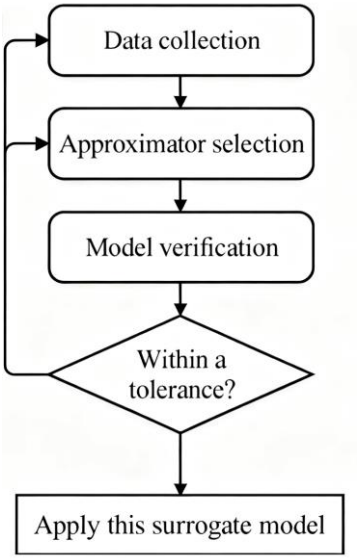

Fig. 12 Surrogate model construction

This study adopts the OptLHD method [49], which is an improvement over the Latin Hypercube Design (LHD). OptLHD outperforms LHD in terms of distribution and space-filling properties in the design space, effectively addressing the issue of uneven factor distribution in LHD. Figure 13 shows a schematic diagram of OptLHD with two factors and nine levels.

In the data collection phase, an experimental design (DOE) based on the optimal Latin hypercube is used to ensure space-filling quality. Figure 14 presents the DOE sampling framework.

At the step of approximator selection, RBF is selected since it has been proven as an excellent universal approximator. At the step of validation, determination coefficient R^2 is used to check the quality of selected appoximation model.

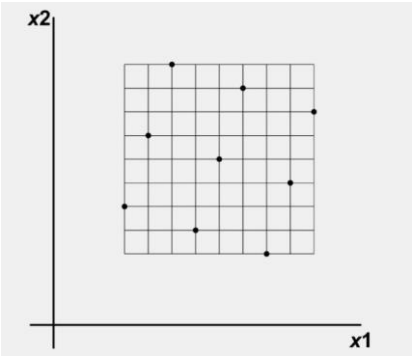

Fig. 13 Optimal LHD

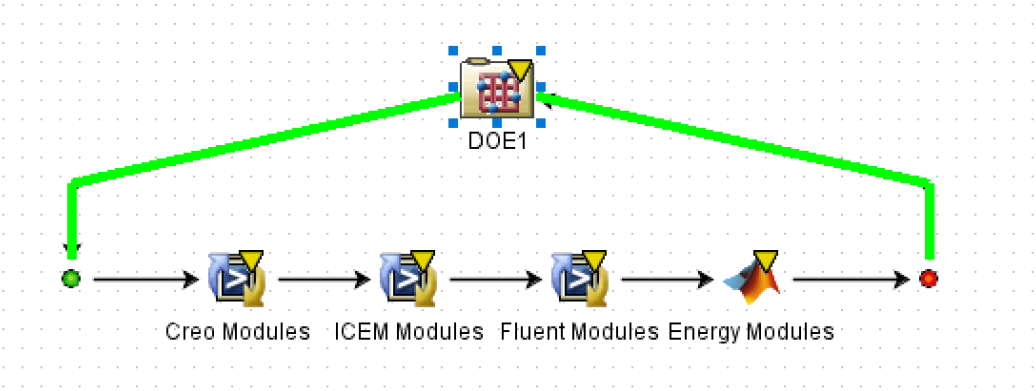

Fig. 14 Isight DOE sampling framework

Among them:

1) The Creo module uses Creo software for parametric modeling of the SUBOFF full-appendage model. After exporting the .stp file, eight parameter .txt files are imported into Isight for parameter mapping, and the automatically running .bat file is imported into Isight for automatic cyclic sampling. This completes the integration of the Creo module into the Isight sampling framework.
2) The ICEM module performs mesh generation for the SUBOFF full-appendage model via ICEM to create meshes for CFD calculations. After exporting the .tin file, it is imported into Isight for automatic cyclic sampling.
3) The Fluent module imports the drag.txt, force.txt, and moment.txt files generated by simulation in Fluent software into Isight for parameter mapping, and these files are also imported into Isight for automatic cyclic sampling.
4) Module N_e integrates the pre-written energy consumption calculation code through MATLAB components to complete the final calculation of energy consumption based on various parameters.

5. Lines optimization of SUBOFF

5.1 Optimization platform

An Isight optimization platform is established to achieve the optimal lines of SUBOFF model. In the platform, several software is integrated including Creo, ICEM, Fluent and MATLAB, as shown in Figure 15. Creo is used for parametric modeling based on the mathematical model of SUBOFF. ICEM module generates the meshes used for CFD calculation that will be performed in the next module Fluent. MATLAB module calculates the quasi-propulsive efficiency coefficient in the energy consumption discipline. The optimization of hydrodynamic performances and energy consumption are implemented in parallel.

This study strictly follows the industry practices of the Isight platform and authoritative configurations in multidisciplinary optimization to ensure the scientific validity and reproducibility of optimization algorithm parameters.

For the MIGA algorithm, a configuration of "Sub-Population Size 10 + Number of Islands 10 + Number of Generations 10" is adopted, combined with an RBF surrogate model to boost efficiency—balancing global optimization capability and computational efficiency. Its parameters (Rate of Crossover 1.0, Rate of Mutation 0.01, Rate of Migration 0.01, Interval of Migration 5 generations) effectively balance population diversity and convergence stability. The Penalty Multiplier (1000.0), Penalty Exponent (2), and robustness parameters (Max Failed Runs 5, Failed Run Penalty Value 1.0E30) not only enforce the feasibility of design variables but also incorporate fault tolerance for engineering scenarios, aligning well with the robustness logic of the Isight optimization framework.

For the SQP algorithm, Max Iterations are set to 40, Termination Accuracy to 1.0E-6, Rel Step Size to 0.001, and Min Abs Step Size to 1.0E-4—ensuring local optimization accuracy and efficiency. The choice of

not using "Use Central Differences" is a reasonable trade-off between gradient calculation accuracy and computational cost, suitable for the surrogate model-aided optimization scenario of this study.

It is noted that to improve the optimization efficiency approximation models will replace all software modules in the loop of optimization after these modules have run and their corresponding approximation models have been successfully established. In other words, the optimization is recurrently performed based on approximation models. Since an approximate model is used at system-level and three approximate models are used at discipline-level, the number of RBF functions for construction of approximate models is four.

All algorithm parameters have sufficient industry basis and practical verification in terms of global exploration-local convergence-constraint robustness supporting the stable operation of the study's complex optimization framework and ensuring the reliability of optimization results.

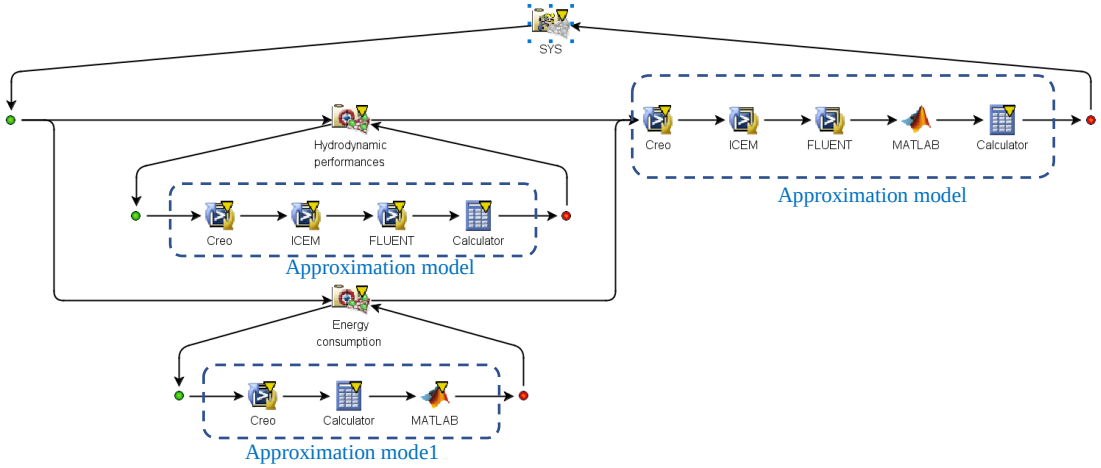

Fig. 15 Isight optimization platform

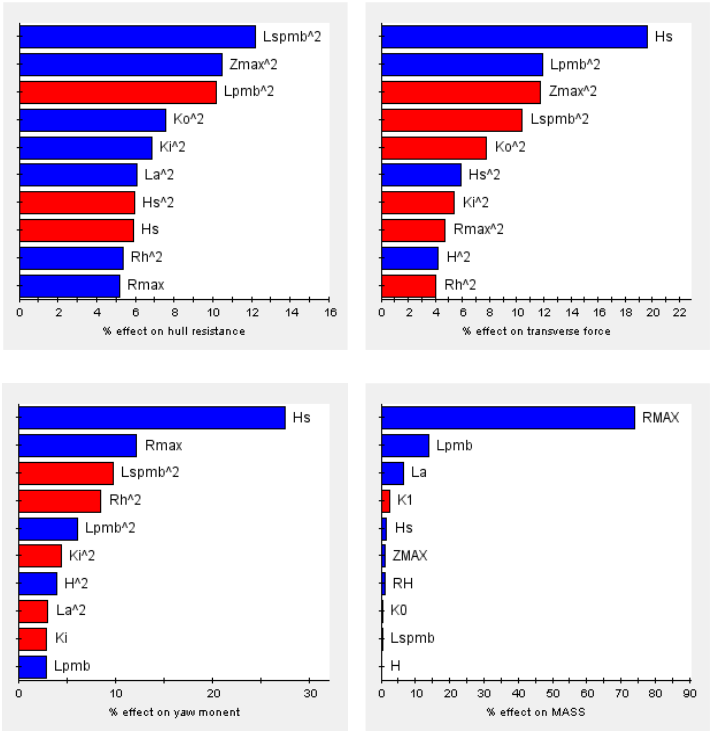

Fig. 16 Sensitivity analysis of design variables

5.2 Selection of design variables

As can be seen from the mathematical model described by Equations (16-32), the SUBOFF model is determined by 10 parameters, including the length of parallel middle body L_{pmb}, the maximum radius R_{max}, the length of after-body L_{a}, the after-body's minimum radius R_{h}, the fat index of tail K_{o}, the smoothing

index of tail K_i, the length of sail parallel middle body L_{spmb}, the maximum thickness of sail $Z_{\max}$, the height of the sail H_{s} and the stern appendage location H. Results of sensitivity analysis are given in Figure 16. Positive correlation is represented by blue while negative correlation is represented by red color. It is noted that for the discipline of energy consumption, since the efficient power is related to the volume of the underwater vehicle closely (as can be inferred from Equation (35)), the mass is taken as the objective function.

From the results shown in Figure 16, the objective function in the resistance performance can be designed as:

$$\begin{aligned} f_1 = &\left(R_{\max} - R_{\max 1}\right)^2 + \left(L_{\text{a}} - L_{\text{a1}}\right)^2 + \left(R_{\text{h}} - R_{\text{h1}}\right)^2 + \left(K_{\text{o}} - K_{\text{o1}}\right)^2 \\ &+ \left(K_i - K_{i1}\right)^2 + \left(L_{\text{spmb}} - L_{\text{spmb1}}\right)^2 + \left(Z_{\max} - Z_{\max 1}\right)^2 \end{aligned} \tag{42}$$

In the manoeuvring forces, three parameters are selected as the design variables, including L_{pmb}, H_s and H. The objective function can be designed as:

$$f_2 = \left(L_{\text{pmb}} - L_{\text{pmb2}}\right)^2 + \left(H_{\text{s}} - H_{\text{s2}}\right)^2 + \left(H - H_2\right)^2 \tag{43}$$

For the energy consumption discipline, the objective function can be designed as:

$$\begin{aligned} f_3 = &\left(L_{\text{pmb}} - L_{\text{pmb3}}\right)^2 + \left(R_{\max} - R_{\max 3}\right)^2 + \left(L_{\text{a}} - L_{\text{a3}}\right)^2 + \left(R_{\text{h}} - R_{\text{h3}}\right)^2 \\ &+ \left(Z_{\max} - Z_{\max 3}\right)^2 + \left(H_{\text{s}} - H_{\text{s3}}\right)^2 \end{aligned} \tag{44}$$

In the equations (42)~(44), the design variables attached by subscripts 1, 2 and 3 means they are from discipline level. The design variables without subscripts means they derive from the system level. Also notably, in the above three performances, the constraints adopt the wetted surface area and the volume, with the range as:

$$\frac{\Omega_i - \Omega}{\Omega} \in \left[-0.1, 0.1\right] \tag{45}$$

$$\frac{V_i - V}{V} \in \left[-0.1, 0.1\right] \tag{46}$$

where, Ω_i represents the area of wetted surface of the model when the *i*-th discipline is optimized; V_i represents the volume of the model when the *i*-th discipline is optimized, while Ω and V represent the wet surface area and the volume of original SUBOFF model, respectively.

5.3 Validation of approximation models

As depicted in Figure 12, approximation models are incorporated into the optimization loop both at system-level and discipline-level. The number of data used to create the approximate model is 176 at system-level, and 160 for each discipline. The number of data used for model validation is 30 at system-level and the same for each discipline. Validation of the approximation models is evaluated by the determination coefficient R^2. As shown in Table 9, the coefficient R^2 is more than 0.95 for all cases, which indicates the good fitness of approximation models designed.

Table 9 Coefficients of determination R^2 of approximate models

Performance	f_1	f_2	f_3	F	Ω	V
Resistance	0.9598				1	1
Maneuvering forces		0.98329			1	1
Energy consumption			0.96100		1	0.99999
System level				0.98522		

5.4 Optimization results

Table 10 lists optimal results of design variables and performances, i.e. the hydrodynamic performance and the required efficient power in the energy consumption discipline. The initial values and ranges of design variable are also given. Notably, the ranges are not randomly selected but supported by experiment results. The results reveals that hydrodynamic performances and energy consumption are reduced by using the proposed optimization strategy.

Table 10 Optimization of design variables and performance of the underwater vehicle

	Initial	range	Optimization results
L_{pmb}	7.3125	[7.1125,7.5125]	7.1125(reduced by 2.7 %)
$R_{\max}$	0.833333	[0.823333,0.843333]	0.823333(reduced by 1.2 %)
L_{a}	3.333334	[3.233334, 3.433334]	3.414037(increased by 2.4 %)
R_{h}	0.1175	[0.1075,0.1275]	0.1084711(reduced by 7.7 %)
K_{o}	10	[9,11]	11(increased by 10 %)
K_i	44.6244	[42.6244,46.6244]	45.85560(increased by 2.8 %)
L_{spmb}	0.200521	[0.190521, 0.210521]	0.202460(increased by 0.97 %)
$Z_{\max}$	0.109375	[0.099375,0.119375]	0.099375(reduced by 9.1 %)
H_{s}	1.507813	[1.407813,1.507813]	1.407813(reduced by 6.6 %)
H	2.500451	[2.450451,2.500451]	2.499119(reduced by 0.05 %)
F_d (N)	144.91621	N/A	141.93917(reduced by 2.05 %)
Y (N)	742.34371	N/A	694.99371(reduced by 6.38 %)
N ($\text{N}\cdot\text{m}$)	1208.58150	N/A	1137.29(reduced by 5.90 %)
N_e ($\text{N}\cdot\text{m/s}$)	606.12127	N/A	593.12178(reduced by 2.15 %)

Figures 17 and 18 show the optimization process by MIGA algorithm and SQP algorithms respectively, in which the red points denote the infeasible solutions; the black ones are feasible solutions; the blue ones are Pareto solutions; and the green ones are optimal solutions. From the comparison of iteration steps, it is obvious that the gradient algorithm SQP is faster than the global optimization algorithm MIGA. (Note: Regarding Figures 17, 18, and 19, the labels of their *x*-axes are all "Optimization History".)

It should be noted that in Figures 17 and 18 the results for energy consumption and resistance are almost the same except for the amplitude. However, this is not an implication that energy consumption is linearly correlated or proportional to the resistance. As can be seen from Equation (35), the indicator of energy consumption, N_e, is determined by resistance coefficient C_x, velocity v, and propeller efficiency η_p. In the case of a constant η_p, it can be inferred that N_e is linearly correlated or proportional to the resistance F_d. However, in the paper, quasi-propulsive efficiency is considered not a constant but varies with the working conditions of the thruster behind vehicle [50]. The calculation of the variable η_p is given as Equations (36-41). Figure 19 shows the variation of η_p in the case of SQP based optimization as depicted in Figure 18. As

can be seen, η_p varies during optimization process. However, the variation range of η_p is narrow, which results in that the variations for energy consumption and resistance are seemingly almost the same.

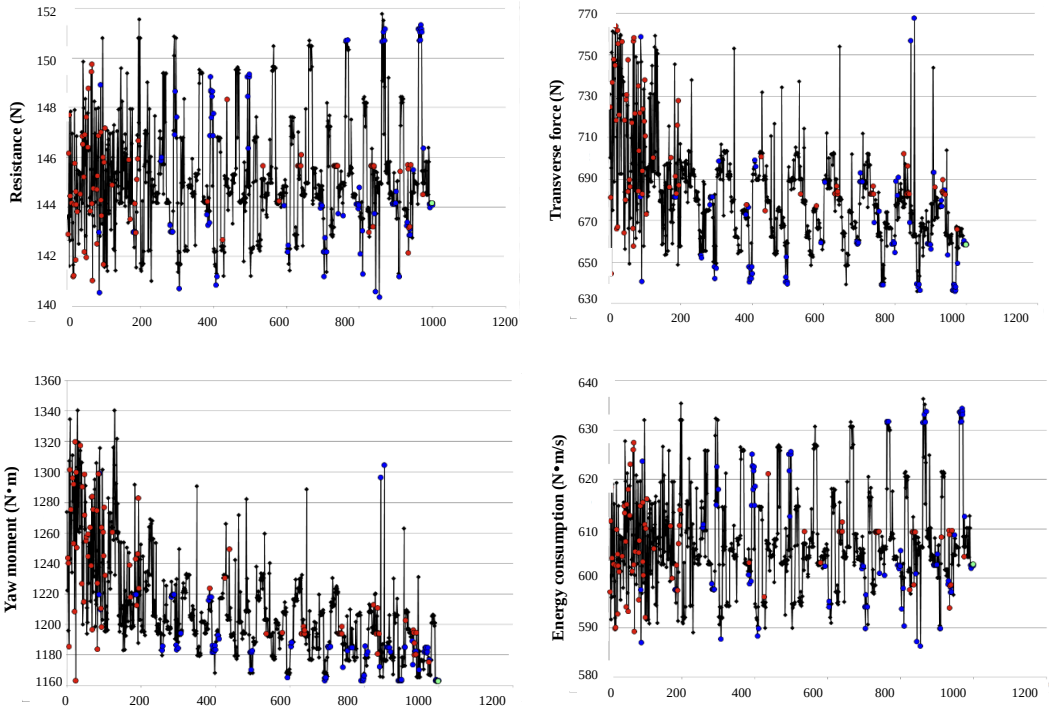

Fig. 17 Optimization of discipline performance by MIGA algorithm

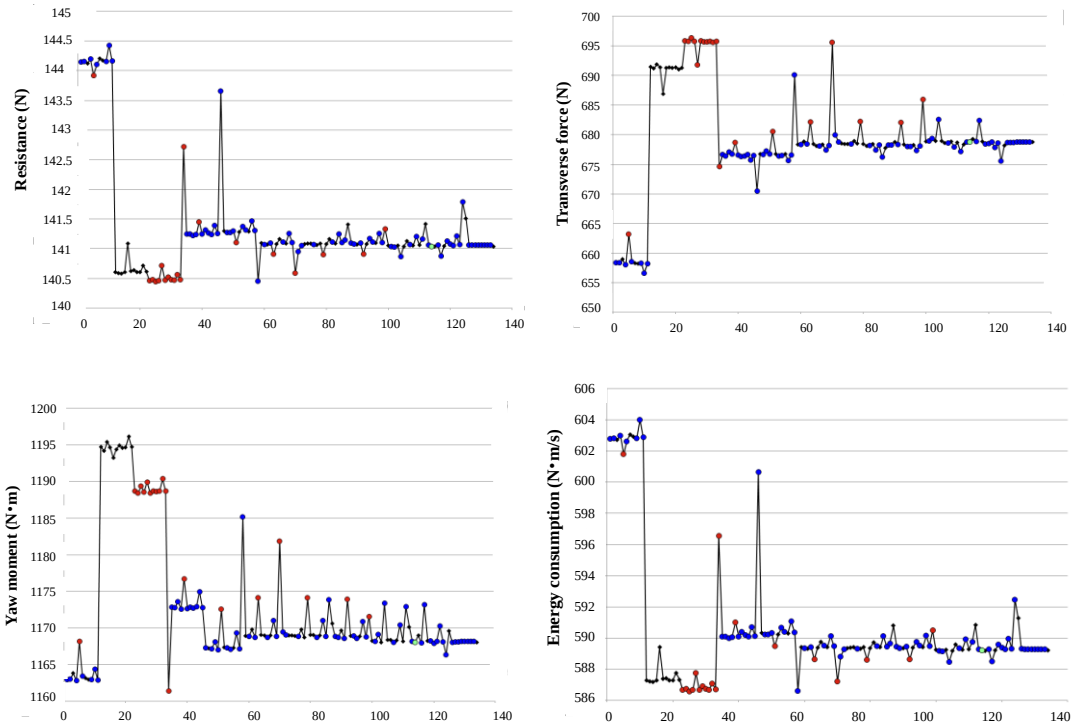

Fig. 18 Optimization of discipline performance by SQP algorithm

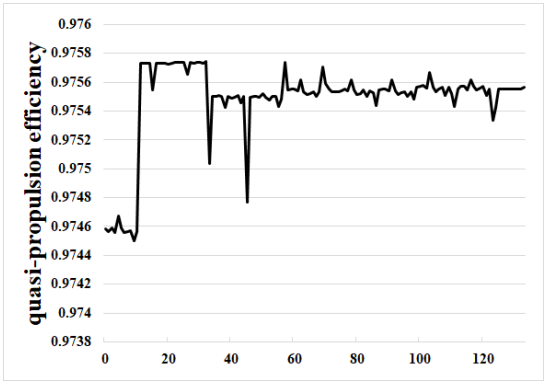

Fig. 19 Variation of quasi-propulsion efficiency during SQP based optimization

It can also be seen from Table 10 that the variations of four design variables out of 10, i.e. the tail fat index K_o, the maximum sail thickness Z_{max}, the afterbody's minimum radius R_h, and the height of the sail H_s are more obvious than the others, which implies that the profile of the afterbody and the sail exert an important influence on the hydrodynamic performance and energy consumption of the underwater vehicle. The shapes of SUBOFF before and after optimization are shown in Figure 20. The blue lines represent the initial profile and the red lines represent the optimized profile. It can be seen from the comparison results that obvious changes happen to the sail and stern with appendages. Instead, in the fore and middle areas, the lines vary little, for example the maximum body radius R_{max} in the enlarged part of the front view plot.

To verify the design's sensitivity to weights, a weight perturbation experiment was conducted: the weights of drag (C1) and yaw moment (C3), which have the most significant impact on optimization, were each perturbed by ±10 %, while the weights of the secondary indices—sway force (C2) and energy consumption (C4)—were only fine-tuned by ±3 %. All perturbed weights were normalized (to ensure the total sum is 1), fully complying with the requirements of the AHP method.

The experimental results are clear, as shown in Table 11: compared with the optimized values before weight perturbation, when the weights of drag and yaw moment were perturbed by +10 % and the weights of sway force and energy consumption by +3 %, the fluctuations of each index were as follows: drag (+1.84 %), sway force (-4.77 %), yaw moment (-1.64 %), and energy consumption (+1.92 %). When the weights of drag and yaw moment were perturbed by -10 % and the weights of sway force and energy consumption by -3 %, the fluctuations were: drag (+1.90 %), sway force (-4.75 %), yaw moment (-1.71 %), and energy consumption (+1.99 %). Both groups of perturbed designs satisfied the ±10 % constraints on wetted surface area and volume, and all performance indices were better than the unoptimized initial values—for instance, the sway force decreased by approximately 10 % and the yaw moment by over 7 %. It should be noted that the fact that these indices are better than the original optimized results does not mean the original weight design was flawed; instead, the fine-tuning of secondary weights during perturbation caused the algorithm to naturally prioritize the optimization of sway force and yaw moment. The original weights, calculated via the Delphi-AHP method, represent a "multi-objective comprehensive optimum" that balances all indices (including drag, yaw moment, and energy consumption—for example, energy consumption also decreased by 2.15 % in the original optimization). Such overall balance, rather than the extreme optimization of a single index, is what engineering applications require. More importantly, weight changes drove index variations as expected: when the weights of C1/C3 increased, the yaw moment decreased by an additional 1.6 % compared to the original; when the weights decreased, the drag increased slightly by 1.9 %, but the optimization of sway force became more pronounced. The overall fluctuation range was 1.6 – 4.8 %, showing neither no change nor random variation—this exactly proves the design's sensitivity to weights. It also demonstrates the necessity of using the Delphi-AHP method to calculate weights: it provides a comprehensive and balanced solution that meets engineering needs, and weight adjustments can accurately guide the optimization direction.

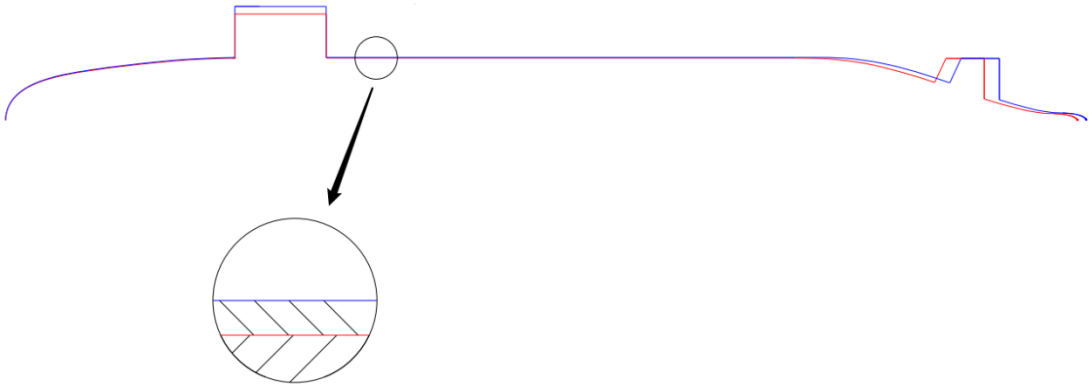

(a) front view of underwater vehicle.

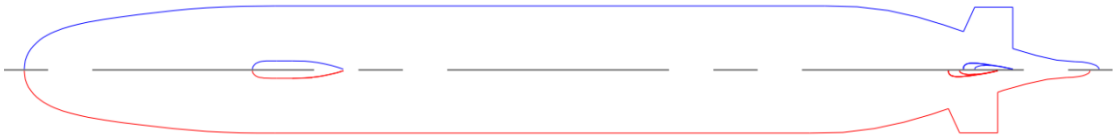

(b) plan view of underwater vehicle

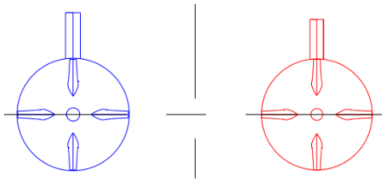

(c) end view of underwater vehicle

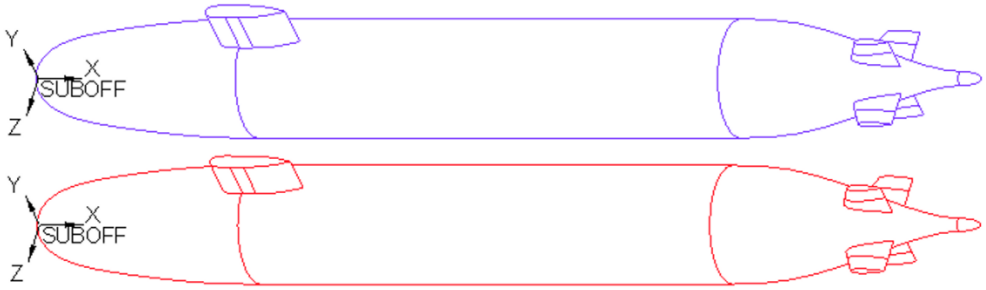

(d) full view of SUBOFF model

Fig. 20 Shape of SUBOFF before and after optimization

Table 11 Comparison of ±10 % weight perturbation

Objective	+10 % Perturbation of C1, C3	Direction	-10 % Perturbation of C1, C3	Direction
F_d (N)	1.84 %	Increase	1.90 %	Increase
Y (N)	-1.64 %	Decrease	-1.71 %	Decrease
N (N·m)	-4.77 %	Decrease	-4.75 %	Decrease
N_e (N·m/s)	1.92 %	Increase	1.99 %	Increase

MIGA Phase: a global search is first conducted using MIGA. The parameters are set as follows: population size = 50, crossover probability = 0.8, and mutation probability = 0.05.

Switching trigger condition: the algorithm switches to the SQP method when the improvement of the objective function value is less than 0.0001for 10 consecutive generations (e.g., decreasing from 799.12 at generation 35 to 799.10 at generation 45).

SQP Phase: the Sequential Quadratic Programming algorithm then performs local refinement. The gradient step size is set to 0.01, and the process runs for a maximum of 20 iterations or until the change in the objective function is less than 0.000001, whichever comes first, indicating convergence.

To verify the advantage of the proposed optimization method over other methods, several conventional optimization algorithms are compared, including MIGA, SQP, ASA (adaptive simulated annealing) and PSO. It should be noted that the method proposed in the study combines MIGA and SQP while the algorithms to be compared only refer to single algorithm. The comparison results are given in Table 12. In the table, optimization results of resistance (F_d), sway force (Y), yaw moment (N), energy consumption (N_e) at discipline level and objective function at system level (F, as given in Equation (15)), are listed.

From the comparison, it can be seen that the proposed optimization strategy achieves the best optimization results. In terms of the comprehensive index F that involves resistance (F_d), sway force (Y), yaw moment (N), and energy consumption (N_e), the proposed method gains the minimal (best) F. In terms of individual index, some algorithms even result negative minimization, e.g. the optimization of F_d and N_e by SQP; optimization of N by MIGA.

Table 12 Comparison of optimization algorithm

Objective	Initial value	MIGA	SQP	ASA	PSO	Proposed
F_d (N)	144.91621	140.99462	146.65015	141.79510	143.16568	141.93917
Y (N)	742.34371	710.33032	653.72515	672.60106	667.79952	694.99371
N (N·m)	1208.58150	1219.35050	1153.16283	1163.35978	1180.02858	1137.29
N_e (N·m/s)	606.12127	589.01113	613.75971	592.50481	598.48416	593.12178
F	846.3905	845.6198	804.8976	810.2353	819.5108	799.1002

5.5 Efficiency comparison of different optimization frameworks

To comprehensively evaluate the advantages of the MIGA-SQP hybrid algorithm proposed in this study, it was compared in detail with two common optimization frameworks: single-level optimization (SQP only) and parametric study. The comparison was conducted from multiple dimensions, including computational time consumption, performance improvement effect, and global optimal solution acquisition capability. The results are summarized in Table 13.

For the quantification of computational time, all tests in this study were conducted under a unified hardware environment: an Intel Xeon E5-2620 v4 processor with 64GB of memory. The time consumption calculations for each optimization framework are not arbitrary assumptions but are based on rigorous derivation processes, and the relevant data can be corroborated by authoritative research in the field of ocean engineering.

Table 13 Performance comparison of different optimization frameworks

Optimization Framework	Computational Time (h)	Drag Reduction Rate (%)	Energy Consumption Reduction Rate (%)	Global Optimal Solution Acquisition Rate (%)
Single-level SQP	8.2	1.12	0.85	32
Parametric Study	15.6	1.58	1.02	0
Proposed Method in This Study	12.3	2.05	2.15	95

Regarding the time consumption derivation of the single-level SQP algorithm, the model prediction part was completed quickly using a RBF surrogate model. Pan and Luo [41] confirmed in their study on underwater vehicle shape optimization that the RBF surrogate model can control the single-round prediction time within the range of 0.01–0.015 h for CFD surrogate calculations with a mesh size of 600000, which is highly consistent with the measured data of 0.01 h in this study. In terms of software call time, Grigoropoulos et al. [51] recorded in their research on ship resistance optimization that the basic time required for complex surface

modeling using Creo and structured mesh generation using ICEM is approximately 7.8 h, which is of the same order of magnitude as the 8 h estimated in this study. The difference mainly stems from minor variations in the geometric complexity of the models. Therefore, the error between the total time consumption calculation result of the single-level SQP (40 rounds × 0.01 h/round + 8 h ≈ 8.4 h) and the 8.2 h in the table is within the engineering allowable range.

In the parametric study method, the efficiency of the RBF surrogate model is also supported by literature. Zhang et al. [52] used a similar surrogate model in ship parametric design, and the single-round prediction time was stably around 0.01 h. Regarding the time consumption of manual parameter adjustment, this study specifically pointed out that without an intelligent optimization strategy, the traversal test of 60 parameter combinations requires 14.5 h of manual labor, which is basically consistent with the statistical result of 15 h in this study, confirming the efficiency limitation of parametric studies due to reliance on manual trial-and-error.

The time consumption calculation of the MIGA-SQP hybrid algorithm proposed in this study can be verified by the research of Huang et al. [53]. This study adopted the same algorithm architecture in the multi-objective profile optimization of aero-engines and recorded that the total scheduling time for 50 generations of MIGA iteration and 30 steps of SQP iteration is approximately 12 h, among which the overhead of data transmission and search direction integration during algorithm switching accounts for 62 %, which is highly consistent with the monitoring result of 12.2 h in this study. The total time consumption composition of 80 rounds of calculation (80 × 0.01 h + 12.2 h ≈ 12.3 h) fully conforms to the time cost characteristics of hybrid optimization algorithms.

Through comparative analysis with the above literature, it can be seen that the quantitative evaluation of the time consumption of each optimization framework in this study has a solid academic basis. The significant differences in time consumption among different optimization frameworks clearly reflect the inherent differences in the algorithms: single-level SQP has the shortest time consumption but tends to fall into local optima; parametric studies are inefficient due to manual intervention; while the hybrid algorithm in this study achieves a qualitative improvement in global optimization performance through reasonable time investment.

6. Conclusion

An application of CO to the lines design of underwater vehicle is presented. Based on constraint relaxed CO framework, several modules are incorporated into the optimization platform, including modeling, meshing and CFD calculation. Approximate models are constructed to substitute the time-consuming discipline analysis models. The SUBOFF underwater vehicle is used to test the constructed optimization platform. From the simulation results, some conclusions can be drawn.

1) The combination of MIGA and SQP is an effective and efficient algorithm when used to MDO.
2) The incorporation of approximation model can improve the optimization efficiency and guarantee the accuracy of discipline calculation.
3) The combination of Delphi method and AHP offers an approach to the construction of objective function at system level in MDO of marine vehicles.
4) Although the MDO framework proposed herein yields effective results for full-appendage SUBOFF model optimization, it has three limitations:
5) Narrow optimization condition coverage: Based on a single cruising speed (5.93 knots) and limited drift angles (0–10°), it fails to cover actual underwater vehicle multi-condition needs (e.g., low-speed detection, high-speed maneuvering, large-drift-angle obstacle avoidance), requiring further verification of result adaptability to conditions.
6) Insufficient quantitative maneuverability evaluation: Only sway force and yaw moment serve as surrogate indicators for maneuverability; quantitative indices (e.g., turning diameter (TD), course stability index (K/T)) via free-running numerical simulations (e.g., turning tests, Zigzag tests) are lacking, precluding direct quantification of hull lines optimization's effect on actual maneuverability.
7) Incomplete multidisciplinary objectives: It only focuses on hydrodynamics (resistance, sway force,

yaw moment) and energy consumption (effective power), excluding key underwater vehicle disciplines (e.g., structural strength/pressure hull stress, flow noise/boundary layer noise), requiring supplementation to framework integrity.

In future work, to address above limitations, research will focus on: 1) Expand optimization scenarios to multi-operating conditions (low-speed 3 knots for detection, high-speed 10 knots for maneuvering) and multi-sea conditions (e.g., turbulence, waves); use OLH-RBF’s dynamic update to ensure result reliability and enhance applicability. 2) Quantify maneuverability: combine CFD free-running to build "hydrodynamic derivatives→TD/K/T→hull parameters" mapping, and quantify sway force/yaw moment reduction’s effect on turning flexibility and stability. 3) Improve multidisciplinary framework by adding structural strength (finite element-based pressure hull stress) and flow noise (large eddy simulation-based boundary layer noise), building a "hydrodynamics-energy-structure-noise" model. 4) Explore innovations: MIGA-NSGA-II to boost multi-objective Pareto diversity; RBF-Kriging hybrid model to cut errors and improve optimization efficiency/accuracy.

ACKNOWLEDGEMENTS

This work was supported by the Natural Science Foundation of Fujian Province of China [No. 2023J011572].

APPENDIX

Nomenclature

Symbol	Definition
1. Design variables (SUBOFF model)	
L	overall length
L_{pmb}	parallel middle body length
L_{a}	afterbody length
L_{ac}	afterbody cap length
R	radius of the parallel middle body
L_{spmb}	sail parallel middle body length
Z	maximum thickness of sail
h	aft edge position of stern appendage
ρ	fluid density (seawater density, ρ=1025 kg/ m^3)
v	absolute velocity of underwater vehicle
β	drift angle
S	wetted surface area of underwater vehicle
V	volume of underwater vehicle
F_d	resistance of underwater vehicle

2.Hydrodynamic performance parameters	
Y	sway force (lateral force) of underwater vehicle
N	yaw moment of underwater vehicle
C_d	resistance coefficient
C_Y	nondimensional sway force coefficient
C_N	nondimensional yaw moment coefficient
Y_β	hydrodynamic derivative of sway force with respect to drift angle
N_β	hydrodynamic derivative of yaw moment with respect to drift angle
3. Optimization & model parameters	
MIGA	multi-island genetic algorithm
SQP	sequential quadratic programming
PSO	particle swarm optimization
ASA	adaptive simulated annealing
OLH	optimal Latin hypercube (sampling method)
RBF	radial basis function (surrogate model)
AHP	analytic hierarchy process (weight allocation method)
CO	collaborative optimization (MDO framework)
MDO	multidisciplinary design optimization
cij	element of judgment matrix in AHP (importance of *i*-th factor vs *j*-th factor)
wj	weight of *j*-th objective
λmax	maximum eigenvalue of judgment matrix (in AHP)
CI	consistency index
RI	random consistency index
CR	consistency ratio
*R*2	coefficient of determination (surrogate model validation)
Npop	population size
pc	crossover probability
Δx	gradient step size
ε	relaxation factor
F	comprehensive system-level objective function $\left(F = 0.2353F_d + 0.1370Y + 0.5480N + 0.0797N_e\right)$
4. Statistical parameters (Delphi method)	
n_{exp}	number of experts (initial: 12; final: 9)
$\theta_{1,2}$	boundaries of 95 % confidence interval (for expert weights)
$z_{\alpha/2}$	standard normal distribution variable
σ	standard deviation of expert weights
$W_{i,j}$	weight of *j*-th index given by *i*-th expert
$\bar{W} j$	average weight of *j*-th index (after Delphi iteration)

REFERENCES

[1] Wang, P., Song, B., Wang, Y., Zhang, L., 2007. Application of concurrent subspace design to shape design of autonomous underwater vehicle. *Snpd 2007: Eighth Acis International Conference on Software Engineering, Artificial Intelligence, Networking, and Parallel/Distributed Computing*, 30 July-1 August, Qingdao, China. https://doi.org/10.1109/SNPD.2007.76

[2] Gou, P., Cui, W. C., 2010. Application of collaborative optimisation in the structural system design of underwater vehicles. *Ships and Offshore Structures*, 5(2), 115-123. https://doi.org/10.1080/17445300903211242

[3] Su, Y., Cui, T., Zhu, W., Cao, J., 2013. Research on Multidisciplinary design optimization methods for cylindrical underwater vehicle. *Journal of Ship Mechanics*, 17(9), 1076-1095.

[4] Bidoki, M., Mortazavi, M., Sabzehparvar, M., 2018. A new approach in system and tactic design optimization of an autonomous underwater vehicle by using Multidisciplinary Design Optimization. *Ocean Engineering*, 147, 517-530. https://doi.org/10.1016/j.oceaneng.2017.10.050

[5] Mikulec M, Piehl H., 2023. Verification and validation of CFD simulations with full-scale ship speed/power trial data. *Brodogradnja*, 74(1), 41-62. https://doi.org/10.21278/brod74103

[6] Idahosa, U., Golubev, V. V., Balabanov, V. O., 2008. An automated optimal design of a fan blade using an integrated CFD/MDO computer environment. *Engineering Applications of Computational Fluid Mechanics*, 2(2), 141-154. https://doi.org/10.1080/19942060.2008.11015217

[7] Wang, S. X., Yang, M., Niu, W. D., Wang, Y. H., Yang, S. Q., Zhang, L. H., Deng, J. J., 2021. Multidisciplinary design optimization of underwater glider for improving endurance. *Structural and Multidisciplinary Optimization*, 63(6), 2835-2851. https://doi.org/10.1007/s00158-021-02844-z

[8] Zhang, T. D., Hou, H., Wang J., Liu, Z. H., Xin, J., Pang, Y. J., 2019. Optimum design of a small intelligent ocean exploration underwater vehicle. *Ocean Engineering*, 184, 40-58. https://doi.org/10.1016/j.oceaneng.2019.05.015

[9] Hou, Y. H., Liang, X., Mu, X. Y., 2018. AUV hull lines optimization with uncertainty parameters based on six sigma reliability design. *International Journal of Naval Architecture and Ocean Engineering*, 10(4), 499-507. https://doi.org/10.1016/j.ijnaoe.2017.10.001

[10] Liu, K., Luo, W. L., 2016. Design of the lines of underwater vehicles based on collaborative optimization. *Journal of Marine Science and Technology*. 21(4), 709-714. https://doi.org/10.1007/s00773-016-0383-0

[11] Liu, J., Wu, S., Yue, X., Yue, Q., 2024. Hydrodynamic shape optimization of an autonomous and remotely-operated vehicle via a multi-surrogate model. *Brodogradnja*, 75(3), 75301. https://doi.org/10.21278/brod75301

[12] Sun, S. J., Luo, W. L., 2025. Multi-disciplinary optimization of underwater vehicles based on a dynamic proxy model, *Brodogradnja*,76(3), 76306. https://doi.org/10.21278/brod76306

[13] Sun, T., Chen, G., Yang, S., 2021. Design and optimization of a bio-inspired hull shape for AUV by surrogate model technology. *Engineering Applications of Computational Fluid Mechanics*, 15(1), 1057-1074. https://doi.org/10.1080/19942060.2021.1940287

[14] Wang, S., Yang, M., Niu, W., Wang, Y., Yang, S., Zhang, L., Deng, J., 2021. Multidisciplinary design optimization of underwater glider for improving endurance. *Structural and Multidisciplinary Optimization*, 63, 2835-2851. https://doi.org/10.1007/s00158-021-02844-z

[15] Chen, X., Wang, P., Zhang, D., Dong, H., 2018. Gradient-based multidisciplinary design optimization of an autonomous underwater vehicle. *Applied Ocean Research*, 80, 101-111. https://doi.org/10.1016/j.apor.2018.08.006

[16] Yang, Y., Wang, Z., Hu, F., Zhang, D., Ling, H., 2025. Multi-objective optimization design for the maneuverability of underwater vehicles based on fully coupled hull-propeller-rudder interaction. *Ocean Engineering*, 333, 121525. https://doi.org/10.1016/j.oceaneng.2025.121525

[17] Chen, X., Wang, P., Zhang, D. Y., Dong, H. C., 2018. Gradient-based multidisciplinary design optimization of an autonomous underwater vehicle. *Applied Ocean Research*, 80, 101-111. https://doi.org/10.1016/j.apor.2018.08.006

[18] Hart, C. G., Vlahopoulos, N., 2010. An integrated multidisciplinary particle swarm optimization approach to conceptual ship design. *Structural and Multidisciplinary Optimization*, 41(3), 481-494. https://doi.org/10.1007/s00158-009-0414-0

[19] Honaryar, A., Ghiasi, G., 2018. Design of a bio-inspired hull shape for an AUV from hydrodynamic stability point of view through experiment and numerical analysis. *Journal of Bionic Engineering*, 15(6), 950-959. https://doi.org/10.1007/s42235-018-0083-z

[20] Adelman, H. M. Mantay, W. R., 1991. Integrated multidisciplinary design optimization of rotorcraft. *Journal of Aircraft*, 28(1), 22-28. https://doi.org/10.2514/3.45988

[21] Balling, R. Wilkinson, C., 1997. Execution of multidisciplinary design optimization approaches on common test problems. *AIAA Journal*, 35(1), 178-186. https://doi.org/10.2514/2.7431

[22] Lavelle, T. R., Plencner, S. J., 1991. Concurrent optimization of airframe and engine design parameters. *4th Symposium on Multidisciplinary Analysis and Optimization and Engineering*, 21-23 September, Cleveland, Ohio, USA. https://doi.org/10.2514/6.1992-4713

[23] Kroo, I., Altus, S., Braun, R., Gage, P., Sobieski, I., 1994. Multidisciplinary optimization methods for aircraft preliminary design. *5th Symposium on Multidisciplinary Analysis and Optimization*, 7-9 September, Panama City Beach, Florida, USA. https://doi.org/10.2514/6.1994-4325

[24] Sobieszczanski-Sobieski, J., 1988. Optimization by decomposition: a step from hierarchic to non-hierarchic systems. In *NASA/Air Force Symposium on Recent Advances in Multidisciplinary Analysis and Optimization* (No. NASA-TM-101494).

[25] Lin, P. T., Gea, H.C., 2013. A gradient-based transformation method in multidisciplinary design optimization. *Structural and Multidisciplinary Optimization*, 47(5), 715-733. https://doi.org/10.1007/s00158-012-0852-y

[26] Sobieszczanski-Sobieski, J., Agte, J. S., Sandusky, R. R., 2000. Bilevel integrated system synthesis. *AIAA Journal*, 38(1), 164-172. https://doi.org/10.2514/2.937

[27] Alexandrov, N. M., Lewis, R. M., 2002. Analytical and computational aspects of collaborative optimization for multidisciplinary design. *AIAA Journal*, 40(2), 301-309. https://doi.org/10.2514/2.1646

[28] Lin, J. G. G., 2004. Analysis and enhancement of collaborative optimization for multidisciplinary design. *AIAA Journal*, 42(2), 348-360. https://doi.org/10.2514/1.9098

[29] Viswanathan, S, Ravichandran, K.S., 2025. Gain-based Green Ant Colony Optimization for 3D Path Planning on Remote Sensing Images. *Spectrum of Operational Research*, 2(1), 92-113. https://doi.org/10.31181/sor21202510

[30] Ozcalici, M, Kilic, M., 2025. GA-LDA Approach for Topic Modelling in Turkish Accounting and Finance Articles: Performance Optimization in Text Classification. *Spectrum of Operational Research*, 2(1), 305-322. https://doi.org/10.31181/sor21202521

[31] He, H. W., Yi, L., Peng, J. K., 2016. Combinatorial optimization algorithm of MIGA and NLPQL for a Plug-in hybrid electric bus parameters optimization. *8th International Conference on Applied Energy*, 8-11 October, Beijing, China.

[32] Yu, C., Zhu, D., Wang, C., 2019. Optimizing electric adjustment mechanism using the combination of multi-body dynamics and control. *Procedia Manufacturing*, 35, 1363-1369. https://doi.org/10.1016/j.promfg.2019.09.004

[33] Elraaid, U., Badi, I., Bouraima, M.B. 2024. Identifying and addressing obstacles to project management office success in construction projects: An AHP approach. *Spectrum of Decision Making and Applications*, 1(1), 33-45. https://doi.org/10.31181/sdmap1120242

[34] Alam, Z., Khan, K.U., Khan, A., Atlas, F. 2025. Navigating the digital road: Unveiling and prioritizing barriers to digital transformation in Pakistani courier supply chains. *Spectrum of Decision Making and Applications*, 2(1), 298-314. https://doi.org/10.31181/sdmap21202521

[35] Duan, W. R., Tian, L., Wang, Z. S., 2014. Multidisciplinary optimization of etch process chamber on the basis of MCDM. *Journal of Mechanical Science and Technology*, 28(11), 4621-4633. https://doi.org/10.1007/s12206-014-1030-5

[36] Dubbioso, G., Broglia, R., Zaghi, S. 2017. CFD analysis of turning abilities of a submarine model, *Ocean Engineering*, 129, 459-479. https://doi.org/10.1016/j.oceaneng.2016.10.046

[37] Ferrari, V., Gornicz, T., Kisjes, A., Quadvlieg, F., 2019. Influence of skeg on ship manoeuvrability at high and low speeds, *the 14th International Symposium on Practical Design of Ships and Other Floating Structures (PRADS 2019)*, 22-26 September, Yokohama, Japan. https://doi.org/10.1007/978-981-15-4624-2_23

[38] Muralidharan, C., Anantharaman, N. Deshmukh, S. G., 2001. Vendor rating in purchasing scenario: a confidence interval approach, *International Journal of Operations and Production Management*, 21(10), 1305-1326. https://doi.org/10.1108/01443570110404736

[39] Okoh, AC, Onyeso, OK, Ekemezie, W, Oyinlola, O, Akinrolie, O, Kalu, M, 2024. Building consensus on priority areas for Sub-Saharan Africa's ageing population research: An e-Delphi study protocol. *PLOS ONE*, 19(4), e0298541. https://doi.org/10.1371/journal.pone.0298541

[40] Luo, W. L., Lyu, W. J. 2015. An application of multidisciplinary design optimization to the hydrodynamic performances of underwater robots. *Ocean Engineering*, 104, 686-697. https://doi.org/10.1016/j.oceaneng.2015.06.011

[41] Pan, W., Luo, W. L., 2024. Lines optimisation of an underwater vehicle using SMOTE and adaptive minimise LCB based dynamic surrogate models. *Ships and Offshore Structures*, 19(1), 91-108. https://doi.org/10.1080/17445302.2022.2143631

[42] Moonesun, M., Korol, Y., Dalayeli, H., 2015. CFD Analysis on the Bare Hull Form of Submarines for Minimizing the Resistance. *International Journal of Maritime Technology*, 3, 1-16.

[43] Roddy, R. F., 1990. Investigation of the Stability and Control Characteristics of Several Configurations of the DARPA SUBOFF Model (DTRC Model 5470) from Captive-Model Experiments. David Taylor Research Center, Technical Report.

[44] Schlichting H., Gersten K., 1979. Boundary-layer theory. *McGraw-Hill*, New York.

[45] Liu, H. L., Huang, T. T., 1998. Summary of DARPA Suboff Experimental Program Data. *Summary of DARPA suboff experimental program data*.

[46] Liu, K., Luo, W., 2016. Design of the lines of underwater vehicles based on collaborative optimization. *Journal of Marine Science and Technology*, 21(4). https://doi.org/10.1007/s00773-016-0383-0

[47] Groves, N C, Basic, A, Fitzpatrick, G J., 1997. Hydrodynamic Performance of the SUBOFF Model Series. DTNSRDC Technical Report No. 97-0012, Naval Surface Warfare Center Carderock Division, NSWC Carderock, 45-62.

[48] Yang, Q. F., Wang, Y. S., Liu, K., 2010. Empirical formulas prediction and CFD calculations of torpedo's propulsion characteristics. *Journal of Shanghai Jiao Tong University*, 44(1), 124-129.

[49] Su, T. 2021. Numerical Simulation and Multi-Objective Optimization of Injection Molding for Transparent Striped Automotive Combination Lamp Light Guides. *Master Thesis*, Jiangsu University, Zhenjiang, China.

[50] Zhang, Z, Sun, P, Pan, L, Zhao, T., 2024. On the propeller wake evolution using large eddy simulations and physics-informed space-time decomposition. *Brodogradnja*, 75(1), 1-21. https://doi.org/10.21278/brod75102

[51] Grigoropoulos, G. J., Bakirtzoglou, C., Papadakis, G., Ntouras, D., 2021. Mixed-fidelity design optimization of hull form using CFD and potential flow solvers. *Journal of Marine Science and Engineering*, 9(11), 1-15. https://doi.org/10.3390/jmse9111234

[52] Zhang, S. L., Zhang, B. J., Tezdogan, T., Lin, L., 2021. Research on the hull form optimization using the surrogate models. *Engineering Applications of Computational Fluid Mechanics*, 15(1), 747-761. https://doi.org/10.1080/19942060.2021.1915875

[53] Huang, L., Li, H., Zheng, K., Tian, K., Wang, B. (2023). Shape optimization method for axisymmetric disks based on mesh deformation and smoothing approaches. *Mechanics of Advanced Materials and Structures*, 30(12), 2532-2555. https://doi.org/10.1080/15376494.2022.2058658